SAND REPORT

SAND 2001-8711
Unlimited Release
Printed January 2002

Investigation of Advanced Power Plants and Multiple Use Applications for Single Occupancy Vehicles

Peter Van Blarigan
Nicholas Paradiso

Prepared by
Sandia National Laboratories
Albuquerque, New Mexico 87185 and Livermore, California 94550

Sandia is a multiprogram laboratory operated by Sandia Corporation, a Lockheed Martin Company, for the United States Department of Energy under Contract DE-AC04-94AL85000.

Issued by Sandia National Laboratories, operated for the United States Department of Energy by Sandia Corporation.

Available to DOE and DOE contractors from
U.S. Department of Energy
Office of Scientific and Technical Information
P.O. Box 62
Oak Ridge, TN 37831

Telephone: (865)576-8401
Facsimile: (865)576-5728
E-Mail: reports@adonis.osti.gov
Online ordering: http://www.doe.gov/bridge

Available to the public from
U.S. Department of Commerce
National Technical Information Service
5285 Port Royal Rd
Springfield, VA 22161

Telephone: (800)553-6847
Facsimile: (703)605-6900
E-Mail: orders@ntis.fedworld.gov
Online order: http://www.ntis.gov/ordering.htm

SAND2001-8711
Unlimited Release
Printed January 2002

Investigation of Advanced Power Plants and Multiple Use Applications for Single Occupancy Vehicles

Peter Van Blarigan
8414 Gas Transfer Systems and Microengineering

Nicholas Paradiso
8119 Technology Applications

Sandia National Laboratories
P.O. Box 969
Livermore, CA 94551-0969

Abstract

Modeling of advanced and conventional drivetrains in a single occupancy vehicle has been undertaken utilizing numerical modeling. The vehicle modeling code Advisor, developed at the National Renewable Energy Laboratory, has shown that high efficiency, low power output hybrid vehicle drivetrains can almost double the economy relative to conventional powertrains. Experimental verification of the high efficiency potential of a free piston based electrical generator at 2 kilowatts output has been accomplished. For the purpose of introducing this class of transportation, however, the low cost and robust construction of the conventional drivetrain may be the logical first choice.

Intentionally Left Blank

Table of Contents

Page

Tables of Figures

Page

List of Tables

This page intentionally left blank

Investigation of Advanced Power Plants and Multiple Use Applications for Single Occupancy Vehicles

Introduction

The concept of a Single Occupancy Vehicle (SOV) greatly reduces the mass and frontal cross section of this transportation option relative to conventional automobiles. As a result, the prime mover will require substantially less output than the typical automobile. In the case of a hybridized drivetrain, a powerplant output of 2 – 6 kilowatts (KW) may be all that is required.

The design and performance prediction of such a vehicle powertrain is undertaken here. Modeling of the powertrain configuration for purposes of comparison of various state of the art hybrid technologies employing fuel cell, microturbine and homogeneous charge compression ignition (HCCI) free piston- power units is accomplished with the use of an existing vehicle modeling code. Diesel and gasoline conventional powertrains are included as a reference to today's production technology.

As in all modeling situations the confidence in the input parameters determine the significance of the results. In the case of a fuel cell considerable experimental verification of performance in the 2 – 6 kilowatt output range exists. However, this option will require hydrogen as a fuel source, and as such will be hard to put to wide scale usage in the near future. For the HCCI free piston and microturbine configurations, which can run directly on gasoline, natural gas or propane, the efficiency of a 2 kilowatt device is difficult to extrapolate.

To assess the performance of a 2 kilowatt microturbine would require an effort clearly beyond the scope of this investigation. The HCCI free piston generator, however, is under development at a 30 kilowatt size at Sandia and as a result it was possible to do combustion performance testing of a 2 kilowatt size generator. Based on these experiments, which constitute the bulk of the effort in this program, the performance potential of a 2 to 30 kilowatt generator can be quite confidently predicted.

2 Kilowatt HCCI Free Piston Investigation

The HCCI free piston generator under development at Sandia for the last 5 years aims to combine the high efficiency of ideal Otto cycles with the low NOx emissions generation of extremely lean combustion. The incorporation of a free piston double-ended configuration with a permanent magnet linear alternator allows for the electronic control of compression ratio, a critical operating parameter for optimized efficiency. Briefly, a double-ended piston oscillates between combustion chambers at each end of the closed cylinder containing the piston. On each stroke the linear alternator is employed to precisely remove (by generating useful electricity) the energy added to the piston from each combustion event. As a result the compression ratio at each end is a function of how much energy is removed, and since the alternator is controlled

electronically a variable compression ratio is achieved with extreme mechanical simplicity. More detail on the configuration and advantages of such a device can be found in Appendix A. The Sandia HCCI free piston generator is being developed at a 30 kilowatt size for application to both full size six passenger hybrid vehicles and stationary power applications. The combustion experiments to measure efficiency and emissions of this new approach have been done at this 30 kilowatt scale, as well as the design of both the two stroke scavenging system and the linear alternator. Scaling of the scavenging parameters and the linear alternator to 2 kilowatts is felt to be fairly confident based on finite element models, but the combustion performance of a greatly reduced size combustion chamber is not as certain. As size is reduced the surface to volume ratio of the combustion chamber increases steadily, decreasing performance due to greater heat loss fraction into the combustion chamber walls. Also, the smaller piston sizes will oscillate at a faster rate than the larger models, perhaps reaching a time limit on ignition. At some point the combustion event will fail to happen at reasonable pressures, and engine operation will not be possible.

Thus experimental measurement of the performance potential of a 2 kilowatt size combustion experiment would provide a valuable bottom end data point to predicting the performance of free piston powerplants between 2 and 30 kilowatts. As in the 30 kilowatt size the approach is to measure the indicated efficiency of a single combustion event, starting from quiescent and fully homogeneous conditions. Indicated efficiency is the pressure/volume work done on the piston divided by the lower heating value of combustion of the fuel – air mixture. The 2 kilowatt size was selected based on the size of the pressure transducer used to measure the cylinder pressure during the test. Experience developing the 30 kilowatt experiment instructed that the full size (12 millimeter diameter) piezoelectric effect pressure transducers developed for engine thermodynamic calculations are the only suitable units with the precision and stability for efficiency calculations. Either the AVL QC42D-X or the Kistler 7061B are suitable when the diaphragm face is coated with Silastic J silicone rubber. The investigation into the performance of these transducers can be found in Appendix A. This appendix contains details of the 30 kilowatt experiment and operating procedures that are relevant to the smaller experiment as well. Differences between the experiments will be explained below.

To accommodate this transducer the diameter of the cylinder was set to 12 millimeters, utilizing the entire transducer as the cylinder head. The maximum stroke is 61mm. Figure 1 shows the combustion experiment. This experimental configuration resulted in an oscillation rate of 190 hertz, approximately five times faster than the 30 kilowatt experiment. Figures 2, 3 and 4 show photographs of the experiment.

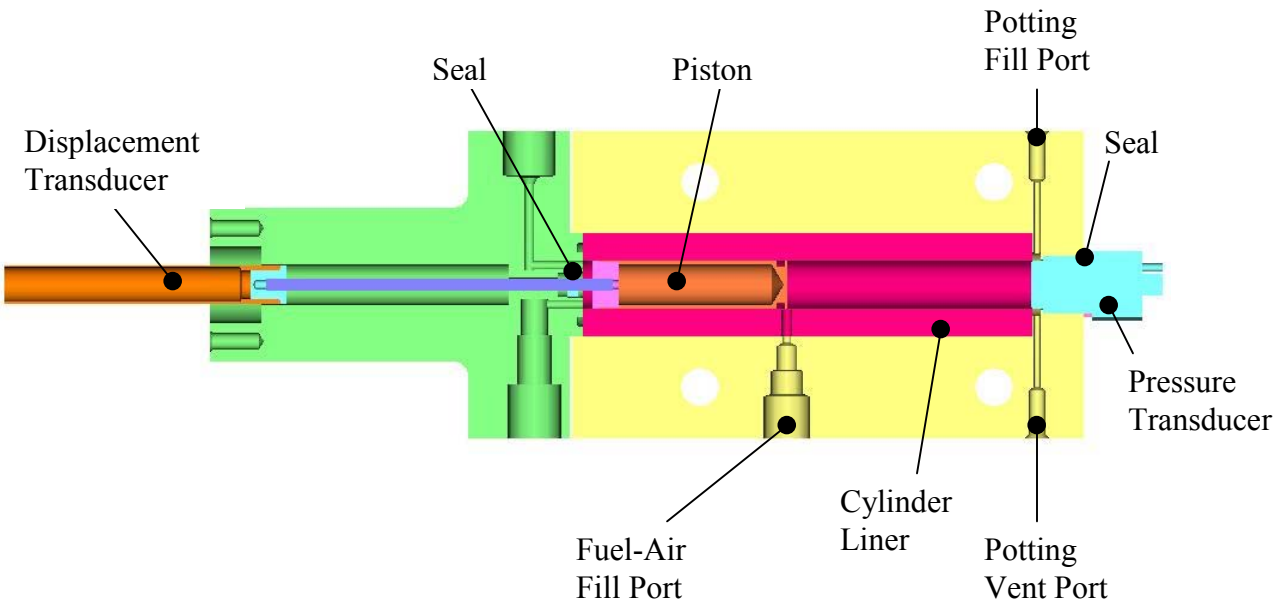

Figure 1: Cutaway Drawing of Small Combustion Experiment.

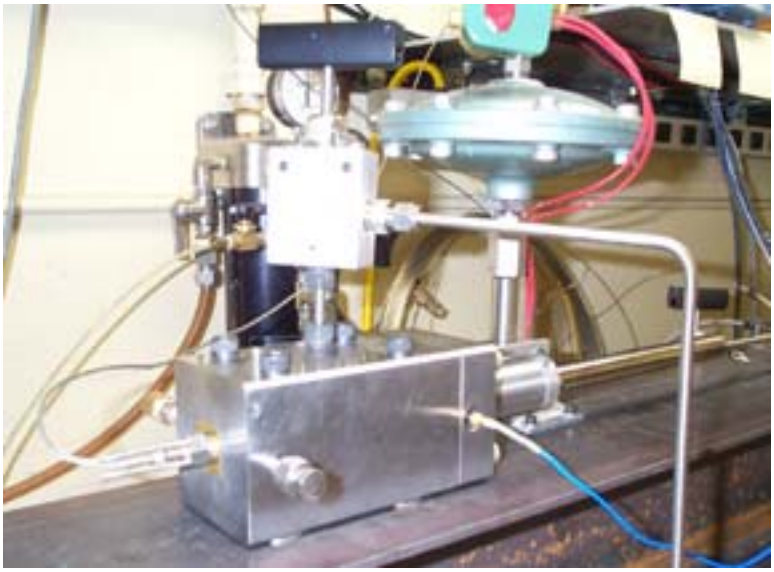

Figure 2: View of combustion end of small scale combustion experiment.

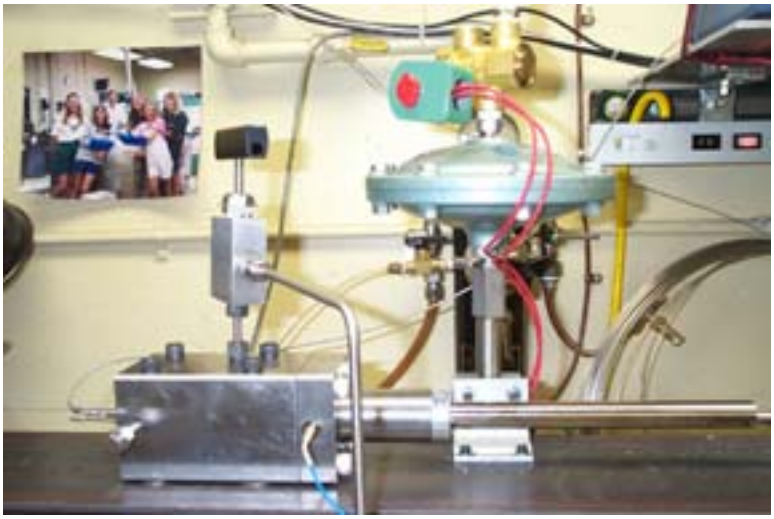

Figure 3: View of side of small scale combustion experiment.

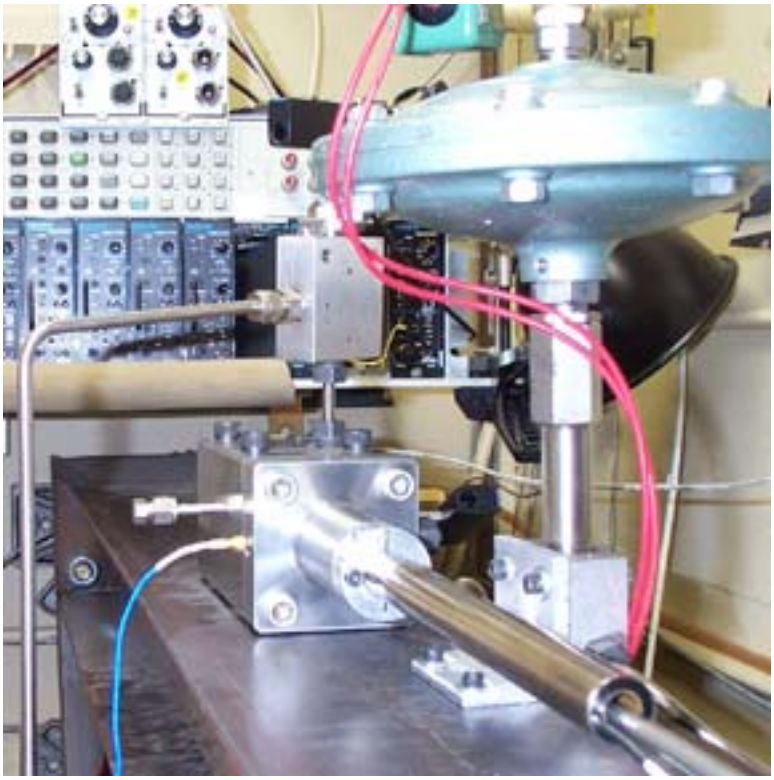

Figure 4: View of driver end of small scale combustion experiment.

In order to reduce the free volume at the top of the cylinder a dummy piston of Teflon was placed in the cylinder 0.1 millimeters from the transducer face. Then Silastic J silicone rubber was injected into the void, coating the transducer and filling any gaps between the transducer body and the cylinder. The port for filling the cylinder with fuel and air was located in the cylinder wall near the bottom of the cylinder. Thus the cylinder volume could be evacuated and backfilled with a premixed fuel and air mixture when the piston was in its starting position. The fuel was premixed and introduced to the cylinder in the same fashion as described in Appendix A.

The high pressure helium driving system designed to provide the force of compression to the piston was modified from the 30 kilowatt design (detailed in Appendix A) to increase the rate of pressure buildup and reduce the volume of gas required. A small volume was separated from the back of the piston by a burst disk modified for minimum internal volume. The small volume was filled through a 100 meter capillary tube with a 0.1 millimeter internal diameter. The capillary acts as a closed valve during the short experiment function time, but an open valve during the relatively long stage when the volume is being pressurized. To conduct an experiment, the fuel – air mixture is placed in the combustion chamber, the high pressure cell evacuated and the small chamber is pumped up slowly (several minutes) until the burst disk fails. The data collection is done on the first stroke, which takes less than 6 milliseconds.

Data was collected as in Appendix A, utilizing the same inductive displacement transducer. The data sample rate was increased to 2 million samples per second to match the increased oscillation rate.

The initial investigation began with air only in the combustion chamber and a burst disk rating of 10,000 pounds per square inch (psi) pressure. The peak pressure recorded during this test would indicate a compression ratio of about 30:1, however the displacement record showed that the piston came within 0.15 millimeters of the cylinder top (pressure transducer face). This number should have been around 1 – 2 millimeters, so it was suspected that the top of the cylinder had some free volume that was not filled in by the Silastic J compound. The cylinder was disassembled and cleaned out of all Silastic except the compound on the face of the transducer. The Teflon insert piston was now placed against the transducer and an epoxy compound (Bondo marine epoxy resin) of very low viscosity was filled in through the potting ports. After potting inspection showed that the epoxy had not covered the transducer face, which remained coated with Silastic J.

The test was repeated and the displacement was as expected. The next tests involved an increase in the burst rating of the disk to 15,200 psi. The increase was intended to generate a higher compression ratio, and a measurement of about 40:1 was recorded.

These initial tests were conducted with an initial pressure of air in the combustion chamber of 760 torr. Since an existing supply of burst disks was available at 15,200 psi it was decided to vary the compression ratio by adjusting the initial combustion chamber charge pressure.

The fuel-air charge tank was filled with a propane-air mixture to an equivalence ratio of 0.334. Equivalence ratio is defined here as the stoichiometric air to fuel ratio divided by the actual air to

fuel ratio. Thus an equivalence ratio of 0.5 has twice the amount of air need for combustion. The 0.334 level was chosen based on experiments with the 30 kilowatt device. This equivalence ratio produced essentially no NOx emissions. Based on increased surface to volume ratio and higher oscillation rate for the 2 kilowatt experiment, it was expected to be able to utilize a higher equivalence ratio for equal NOx control. However, we were not able to measure the NOx from such a small gas sample with our existing instruments and will have to develop alternate methods.

The results for several key tests are shown in Table 1. The first two tests listed did not initiate, so the initial loading pressure was reduced to increase the peak compression ratio. The next two tests, at equivalence ratio of 0.334 and initial pressure of 600 torr, did initiate and produced indicated efficiencies of 40 and 36 percent. After several more similar results it was decided to increase the equivalence ratio to see if efficiency would change. Such an investigation with the 30 kilowatt experiment did show that efficiency trails off when the equivalence ratio becomes very low.

The last test in Table 1 is at an equivalence ratio of 0.679 and an initial fuel – air pressure of 632 torr. This test produced a healthy pressure rise and an indicated efficiency of 56%. Following two tests at these conditions the pressure transducer was recalibrated and found to be working accurately. Pressure and displacement versus time plots for this last test are shown in Figure 5, while Figure 6 shows a log-log plot of the data. The ideal Otto cycle shape of the plot (see Appendix A) is evident.

Table 1: Summary of small scale combustion experiment results.

Test	Fuel	Equivalence Ratio	Initial Pressure (torr)	Efficiency (%)	Burst Disk Pressure (psi)	Peak Pressure (psi)
ss3	propane	0.334	763	-7	15200	2035
ss4	propane	0.334	739	-7	15200	1792
ss5	propane	0.334	599	40	15200	4292
ss6	propane	0.334	600	36	15200	4746
ss8	propane	0.679	632	56	15200	7076

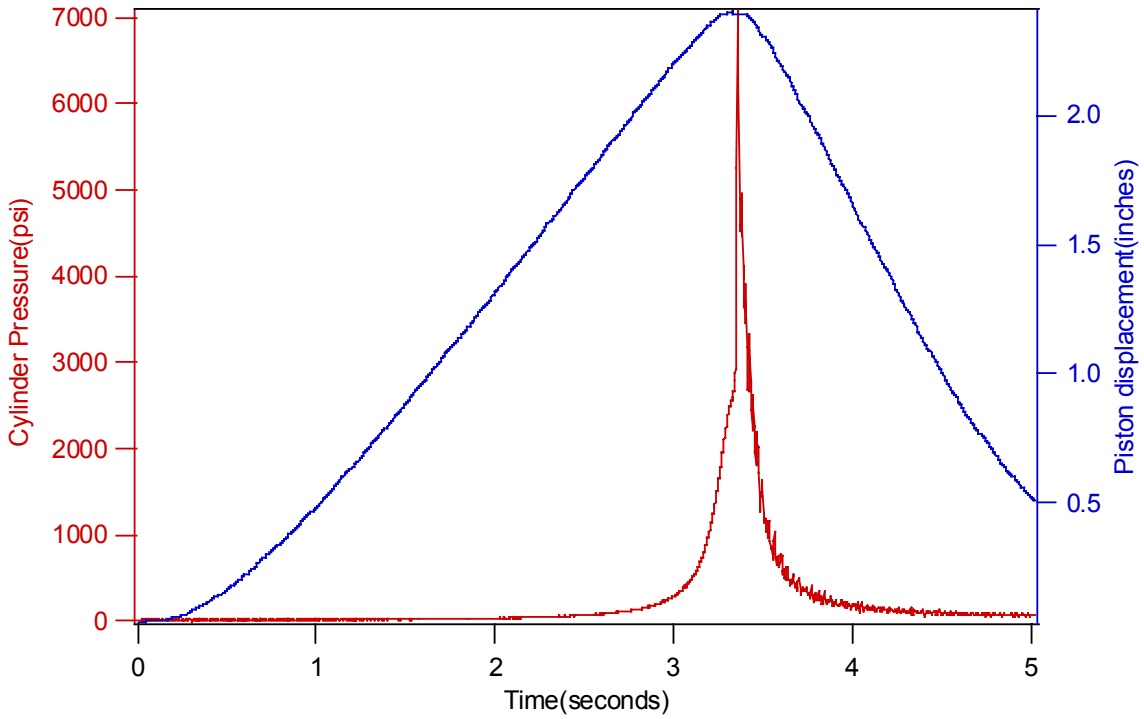

Figure 5: Pressure and piston displacement vs. time for small scale combustion experiment.

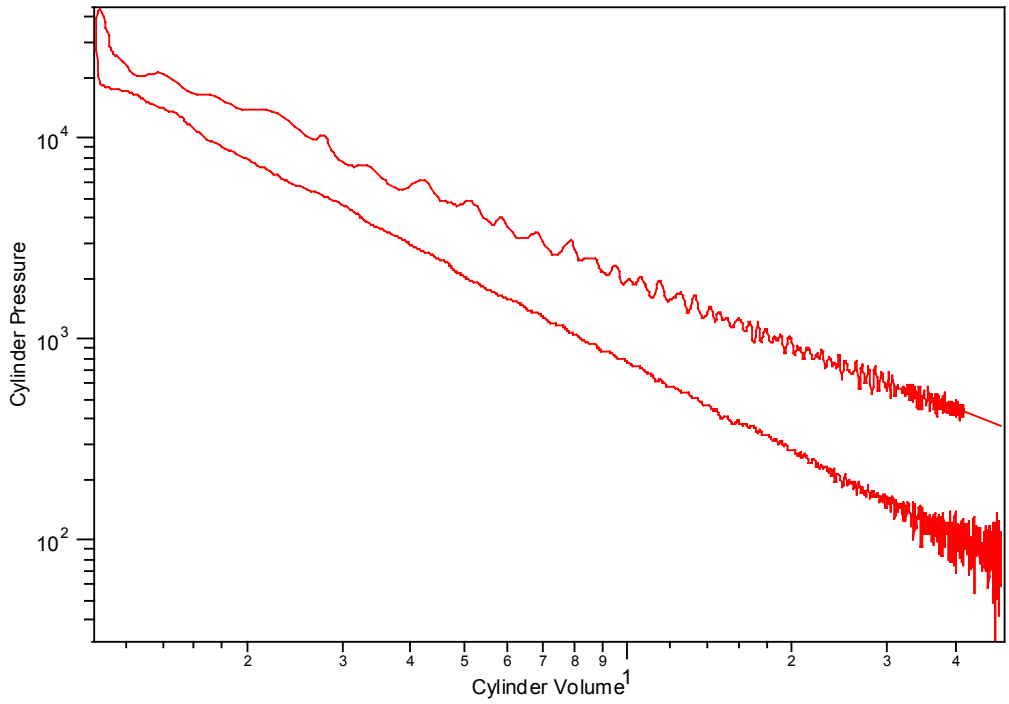

Figure 6: Log-Log plot of cylinder pressure vs. cylinder volume for small scale combustion experiment.

This last test was very encouraging and answers the question posed initially: Can the 30 kilowatt efficiency be extrapolated to smaller power levels? Based on this investigation it appears that efficiency for a free piston HCCI generator can be held constant from 30 to 2 kilowatts for modeling input.

Vehicle Description

The vehicle modeled was a Sparrow Personal Transit Module (PTM) manufactured by Corbin Motors of Hollister California. The vehicle is pictured in Figure 7. The Sparrow is a single passenger vehicle designed primarily for commuter and inner city use. The base vehicle for this study is the standard electric version of the Sparrow. The Sparrow is a three-wheeled vehicle that qualifies for registration as a motorcycle. It is powered by a 31 kW electric motor driving a single rear wheel. The motor is energized by thirteen Optima Spiral Wound lead-acid batteries connected in series with a nominal voltage of 156 volts, and a capacity of sixty amp-hours. The batteries provide for a stated range of thirty to fifty miles. The vehicle has a wheelbase of sixty-one inches, a height of fifty-seven inches, and a curb weight of thirteen hundred fifty pounds. The Sparrow specifications are listed in Table 2.

Figure 7: Sparrow electric vehicle.

Table 2: Sparrow Specifications.

Width	48 inches
Length	96 inches
Weight	1350 pounds
Wheelbase	61 inches
Motor	Advanced DC Motors 31 kW
Batteries	Optima Spiral Wound D900M lead/acid
Battery Pack	13 batteries - 156 volts
Battery Pack Weight	598 pounds
Battery Capacity	60 amp/hr @ 20 hr rate
Top Speed	70 mph
Brakes	3 wheel disc
Tires	155-80-13
Stated Range	30 -60 miles
Accessories	power windows/stereo/heater
Accessory Load	250 Watts

Modeling

All of the modeling was done using the National Renewable Energy Laboratories (NREL) ADvanced VehIcle SimulatOR (Advisor) vehicle modeling software. The Advisor program is a set of modeling files that are used with Matlab and Simulink for analysis of the performance and fuel economy of conventional, electric, and hybrid vehicles. Advisor allows for changing vehicle parameters by the scaling of a built in set of vehicle components (engines, generators, motors), or by the user developing his own vehicle components. The built in components are scaled on the setup page. The user components are developed from text files that set the parameters for the desired component. User developed components are added to the standard Advisor components on the first setup page.

Nine vehicle configurations were modeled on the standard Sparrow chassis. The base vehicle was the standard electric Sparrow. This base vehicle was modified into a series hybrid powered by fifteen and four kilowatt turbines, four, fifteen, and twenty kilowatt hydrogen fuel cells, a four kilowatt free piston-linear alternator series hybrid, a conventional fifteen kilowatt gasoline engine, and a conventional fifteen kilowatt diesel engine. The different models are summarized in Table 3.

Table 3: Modeled vehicle configurations.

Vehicle	Vehicle Weight	Drivetrain	IC Engine		Electric Motor	Batteries	
	(kg)		Type	(kW) / Efficiency (%)	(kW)	Voltage/ Capacity (Ah)	Battery Mass (kg)
base	616	electric vehicle	none	n/a	31	13.2 / 20	256
turbine_15kw	414	series hybrid	turbine	15 / 28	15	13.2 / 2	8.5
turbine_4kw	371	series hybrid	turbine	4 / 25	15	13.2 / 2	8.5
fuel_cell_4kw	421	fuel cell-hydrogen	none	4 / 50	15	13.2 / 2	8.5
fuel_cell_20kw	483	fuel cell-hydrogen	none	20 / 50	15	13.2 / 2	8.5
fuel_cell_15kw	459	fuel cell-hydrogen	none	15 / 50	15	13.2 / 1	4.3
free_piston_4kw	371	series hybrid	free piston	20 / 48	15	13.2 / 2	8.5
conventional_gas 15kw	499	conventional	conventional	15 / 31	n/a	n/a	n/a
conventional_diesel 15kw	494	conventional	conventional	15 / 34	n/a	n/a	n/a

All of the hybrid, electric, and fuel cell vehicles used the same Advanced DC Motors electric motor. The standard Sparrow used a thirty one kilowatt motor. The motors for the fuel cell and hybrid vehicles were scaled to 15 kW. The scaling was done by Advisor and maintains the same efficiency as the original motor, but lowers the torque output across the rpm range to achieve the desired power output.

All vehicles used the same tires, wheels, battery pack voltage, electric accessory load, drag coefficient, and base vehicle weight and dimensions. These vehicle constants are listed in Table 4. The power train control for the series hybrid was handled by a modified version of the Advisor series power train controller that kept the batteries between sixty and eighty percent charged. The power train control for the base electric and conventional vehicles was handled by the stock versions of the corresponding Advisor vehicle controllers.

Table 4: Vehicle constants.

Width	48 inches
Length	96 inches
Wheelbase	61 inches
Battery Pack	13 batteries - 156 volts
Brakes	3 wheel disc
Tires	155-80-13
Accessories	power windows/stereo/heater
Accessory Load	250 Watts

All of the hybrid, electric, and fuel cell vehicles used the same Optima Spiral Wound D900M batteries as used by the Corbin factory. The battery packs for the hybrid and electric vehicles were modeled as separate files for each battery power output level. Battery capacities of one to one hundred and twenty amp-hour capacity were modeled. The battery weights were scaled linearly to correspond to the battery power output. That is a base battery of sixty amp-hour capacity weighs twice as much as a thirty amp-hour capacity battery. Only the final battery selections used for each vehicle are shown in Table 3.

Fuel Cell Vehicles

Three fuel cell vehicles were modeled. They were all derived from an Argonne National Laboratory fifty kilowatt ambient pressure hydrogen fuel cell system. The basic fuel cell was scaled to twenty, fifteen, and four kilowatt outputs. The fuel cell weights were scaled linearly to correspond with the reduction in output power. The fuel cell vehicle weight was increased an extra fifty kilograms to simulate the weight of the hydrogen fuel tank. The batteries for the fuel cell vehicle were scaled from the Optima sixty amp-hour batteries used in the electric vehicle. The total number of batteries was kept at thirteen as in the base vehicle to maintain the design voltage for the electric motor. The battery weight was scaled linearly corresponding to the battery output. The transmission for the fuel cell vehicles was the same single speed transmission used for the base electric vehicle. This transmission was configured for an efficiency of 97%. The vehicle weight was the sum of the base vehicle weight plus the battery pack, fuel cell, transmission, and fuel tank weights.

Turbine Vehicles

Two turbine powered series hybrid vehicles were modeled. The turbine output was scaled to twenty and eight kilowatts. The turbines were modeled using Advisor's constant power output engine model. This model allows for the specification of the engine efficiency and power output level. The model automatically scales the weight of the engine for the selected power output. The battery packs for the turbine vehicles were scaled from the Optima sixty amp-hour batteries used in the electric vehicle. The total number of batteries was kept at thirteen as in the base

vehicle to maintain the design voltage for the electric motor. The battery weight was scaled linearly corresponding to the battery output. The transmission for the turbine vehicles was the same single speed transmission used for the base electric vehicle. This transmission was configured for an efficiency of 97%. The vehicle weight was the sum of the base vehicle weight plus the battery pack, turbine, transmission, and fuel tank weights.

Conventional Vehicles

Two conventional vehicles were modeled. One fifteen kilowatt gasoline and one fifteen kilowatt diesel. The gasoline engine was a scaled version of General Motors 41kW 1.0L Geo Metro engine. The output was scaled by Advisor after setting the power output and efficiency to the desired levels. The transmission for the gasoline vehicle was a stock transmission from Advisor for spark ignition engines. The transmission has five speeds with fifth being an overdrive. The transmission had an efficiency of 91%. The diesel engine was a scaled version of Advisor's built in 37 kW 1.47 L 4-cylinder, naturally aspirated direct injection diesel engine with high swirl single hole injection nozzle. The scaling was done by Advisor after setting the power output and efficiency to the desired levels. The transmission for the diesel vehicle was a stock transmission from Advisor for compression ignition engines.. The transmission has five speeds with fifth being an overdrive. The transmission had an efficiency of 94%. The vehicle weights were the sum of the base vehicle weight plus engine and transmission.

Free Piston Vehicle

A free piston – linear alternator series hybrid drive train was modeled using data from combustion experiments at Sandia National Laboratories. The free piston engine- linear alternator combination was run with propane using a total efficiency of 48% for the four kilowatt unit. This efficiency is from an engine efficiency of 53% with a linear alternator efficiency of 90%. This vehicle used the Advanced DC Motors 31 kW motor scaled to 15kW, with the battery pack set to a two amp-hour capacity. Both the motor and battery weights were scaled linearly to their power outputs. The transmission for the free piston vehicles was the same single speed transmission used for the base electric vehicle. This transmission was configured for an efficiency of 97%. The vehicle weight was the sum of the base vehicle weight plus the battery pack, free piston-linear alternator unit, transmission, and fuel tank weights.

Test Cycles

Two test cycles were performed for each vehicle. The test cycles used were the Urban Dynamometer Driving Schedule (UDDS) and the Highway Fuel Economy Test (HWFET).

The HWFET driving cycle is used to simulate highway driving and estimate typical highway fuel economy. The official test consists of a warm-up phase followed by a test phase. In ADVISOR the warm up phase is replaced by starting the vehicle with hot initial conditions. A top speed of

60 mph is reached with an average speed of 47.6 mph. The test runs for 765 seconds. A graphic representation of the cycle is shown in Figure 8.

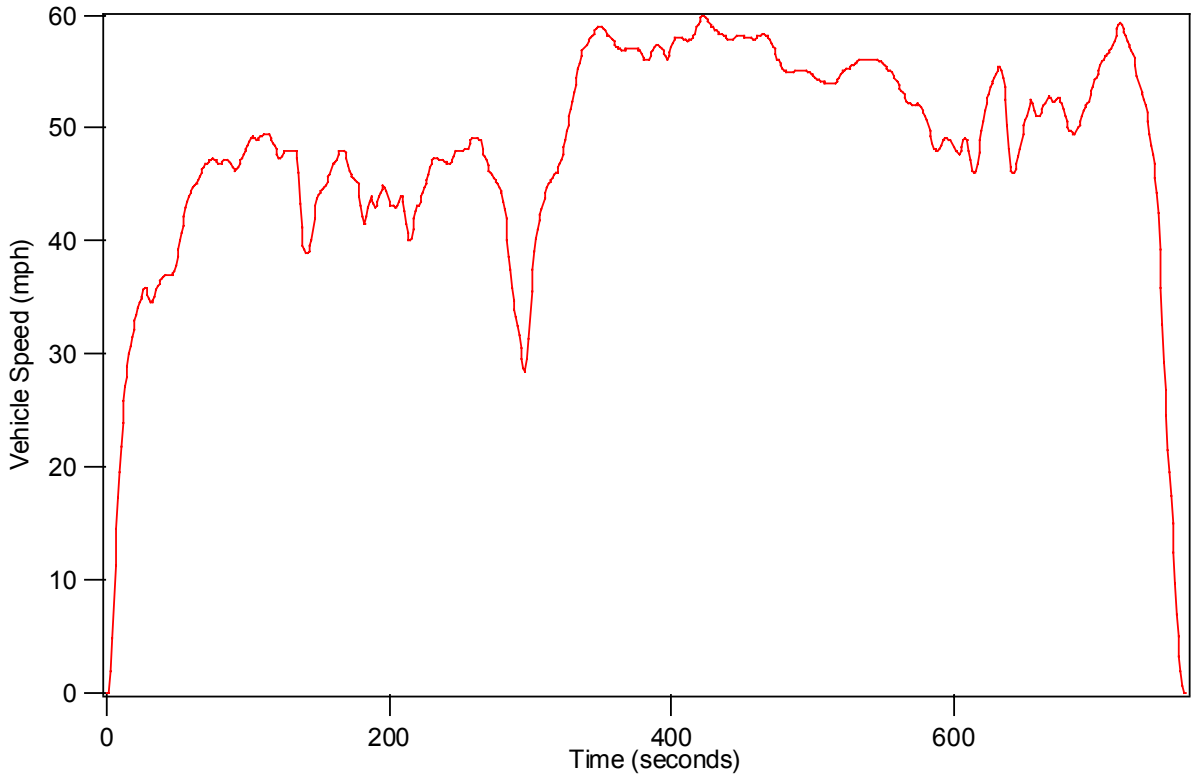

Figure 8: Highway Federal Emissions Test (HWFET).

The UDDS driving cycle is used to simulate city driving and is commonly called the city test or EPA II. It is the equivalent of the first two bags of the Federal Test Procedure (FTP-75). The test runs for 1369 seconds and a maximum vehicle sped of 59 mph is reached with the majority of the test being stop and go driving at less than 35 mph. A graphic representation of the cycle is shown in Figure 9.

Vehicle Performance Tests

In addition to the driving cycle tests all of the modeled vehicles were run through acceleration and gradeability tests. The acceleration tests run were zero to sixty mph, forty to sixty mph acceleration, zero to eighty mph, maximum acceleration, distance in five seconds, and quarter mile performance. Maximum vehicle speed was also tested. The gradeability test was used to determine the maximum grade the vehicle could climb while maintaining fifty mph for thirty seconds.

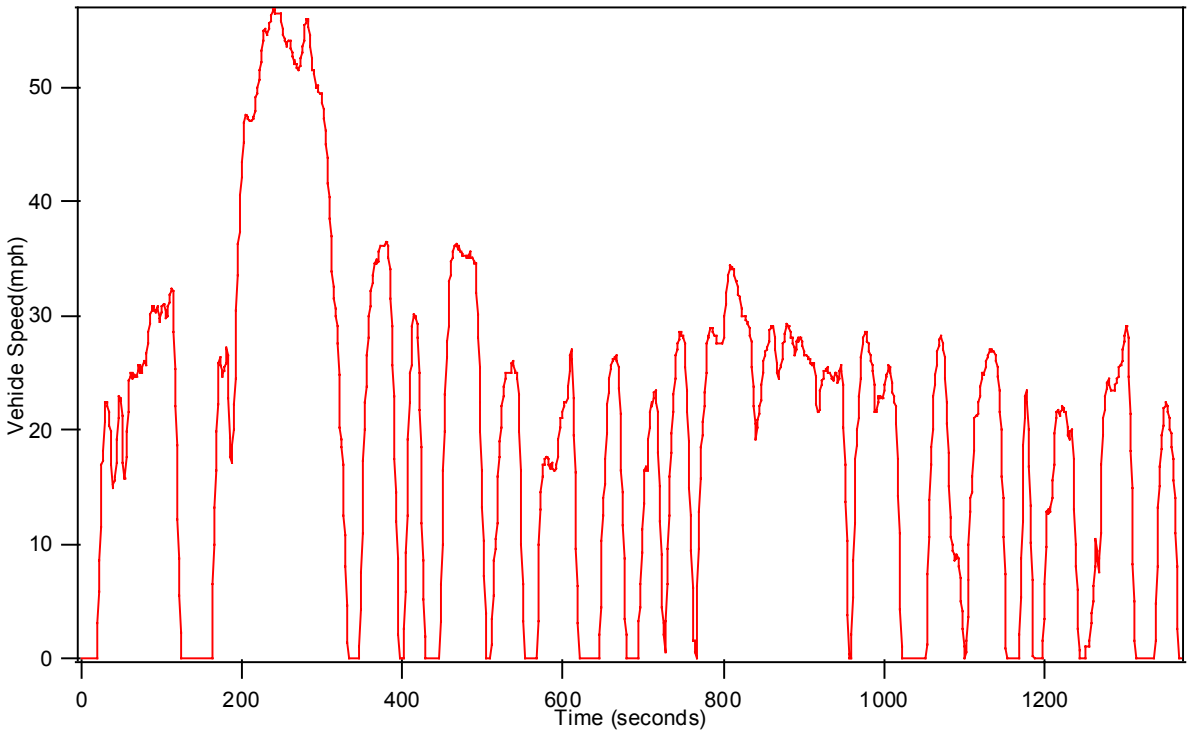

Figure 9: Urban dynamometer driving schedule (UDDS) test.

Results

A summary of the vehicle performance for the testing is presented in Table 5 and Figures 10 through 14.

In Figure 10 the vehicle mileage for the HWFET cycle is shown. The fuel cell and free piston vehicles are at the top of the field being within one percent of each other, with the fuel cell having a slight edge at 236 mpg as compared to the free piston's 233 mpg. This is due to their higher efficiencies as compared to the other engines.

The vehicle mileage for the UDDS cycle is shown in Figure 11. In this test the free piston vehicle bests the fuel cell vehicle by one percent (166 mpg vs. 164 mpg).

Vehicle acceleration from zero to sixty mph is shown in Figure 12. The free piston vehicle has the quickest time here as its lighter weight gives it the advantage.

Figure 13 shows the vehicle times in a quarter mile acceleration test. In this test the free piston and the turbine are the quickest with the free piston having a 1.5% lead. Again this performance edge for these two vehicles is due to their lighter weight.

In Figure 14 the results of the gradeability tests are shown. This test favors a vehicle with a high power to weight ratio. Here the 15kW turbine is able to sustain the 55 mph at the steepest grade.

Table 5: Vehicle performance.

Configuration	Test Cycle	Battery Initial	Fuel Economy	Performance							Max Grade
		SOC		0-60 mph	40-60 mph	0-85 mph	Max Accel	Distance in 5s	1/4 mile	Max Speed	@ 55 mph
		(%)	(mpg)	(s)	(s)	(s)	(ft/s2)	(ft)	(s)	(mph)	(%)
base(ev)	UDDS	1	236.2	17.7	9.3	36.3	17.8	136.2	21.1	98.4	9.7
base(ev)	HFET	1	338.3	17.7	9.3	36.3	17.8	136.2	21.1	98.4	9.7
turbine 4kw	HFET	0.8	111	13.2	7.1	27.7	16.4	156.9	19.1	98.2	11.8
turbine 4kw	UDDS	0.8	78.9	12.6	6.8	26.4	17.3	161.8	18.8	98.2	11.8
turbine 15kw	HFET	0.8	106.5	13.9	7.5	29.4	15.5	151.1	19.4	98.3	11.8
turbine 15kw	UDDS	0.8	75.7	13.9	7.5	29.4	15.5	151.1	19.4	98.3	11.8
fuel_cell 4kw	UDDS	0.8	164.1	14.2	7.6	29.9	15.2	149.5	19.5	98.3	11.6
fuel_cell 4kw	HFET	0.8	236.2	14.2	7.6	29.9	15.2	149.5	19.5	98.3	11.6
fuel_cell 15kw	UDDS	0.8	146.6	15.3	8.3	32.5	13.9	141.3	20.1	98.3	10.5
fuel_cell 15kw	HFET	0.8	209.9	15.3	8.3	32.5	13.9	141.3	20.1	98.3	10.5
fuel_cell 20kw	HFET	0.8	190.5	16.1	8.7	34.2	13.2	136.5	20.4	98.3	9.9
fuel_cell 20kw	UDDS	0.8	132.1	16.1	8.7	34.2	13.2	136.5	20.4	98.3	9.9
free_piston 4kw	UDDS	0.8	166.1	12.6	6.8	26.4	17.3	161.8	18.8	98.2	8
free_piston 4kw	HFET	0.8	233.8	12.6	6.8	26.4	17.3	161.8	18.8	98.2	8
conventional gas_15kw	UDDS	n\a	84.5	23.5	10.8	45.2	8.2	53.5	24.8	106.8	10.6
conventional _gas_15kw	HFET	n\a	128.1	23.5	10.8	45.2	8.2	53.5	24.8	106.8	10.6
conventional diesel_15kw	UDDS	n\a	81.4	22.7	11	44.1	6.8	77.7	24	115.8	11
conventional diesel_15kw	HFET	n\a	156.7	22.7	11	44.1	6.8	77.7	24	115.8	11

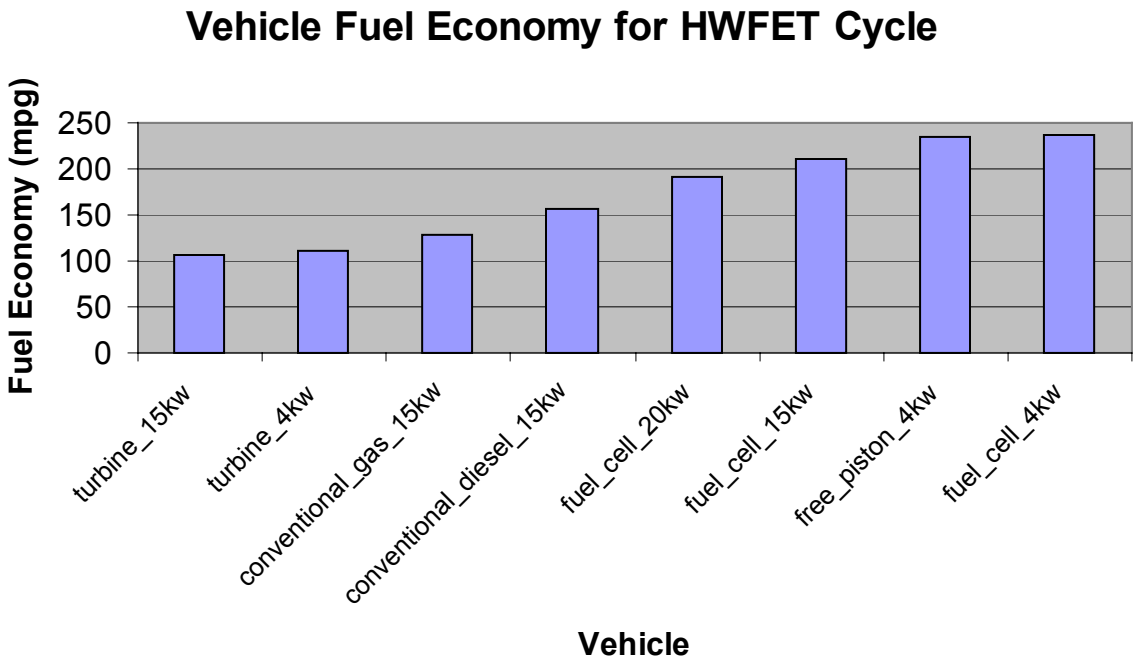

Figure 10: Vehicle Fuel Economy for HWFET Cycle.

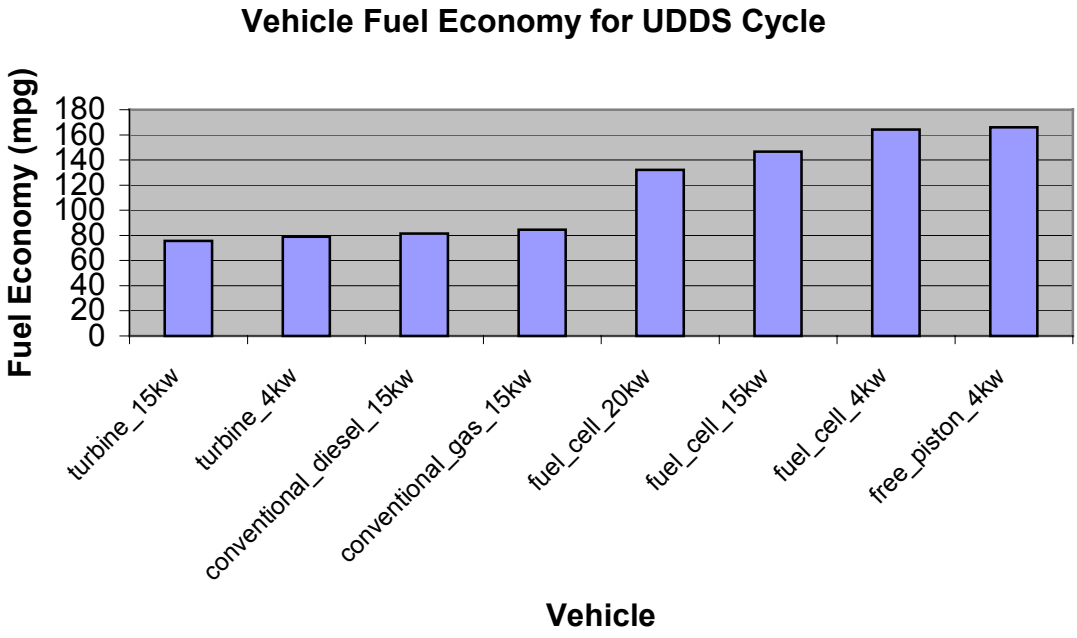

Figure 11: Vehicle Fuel Economy for UDDS Cycle.

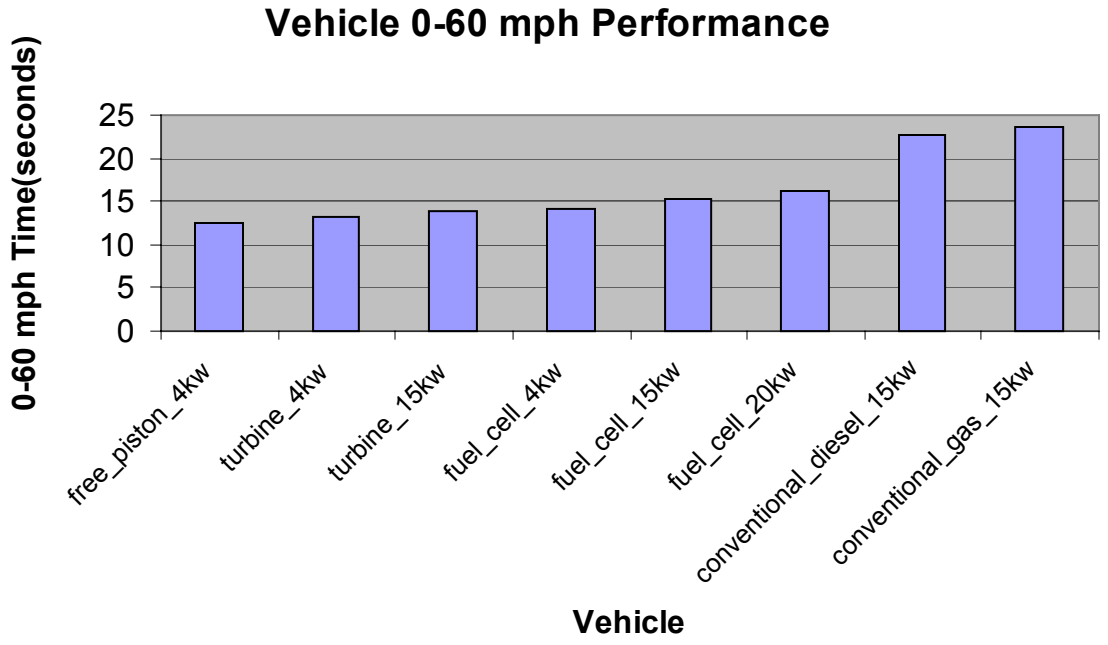

Figure 12: Vehicle 0 to 60 mph Performance.

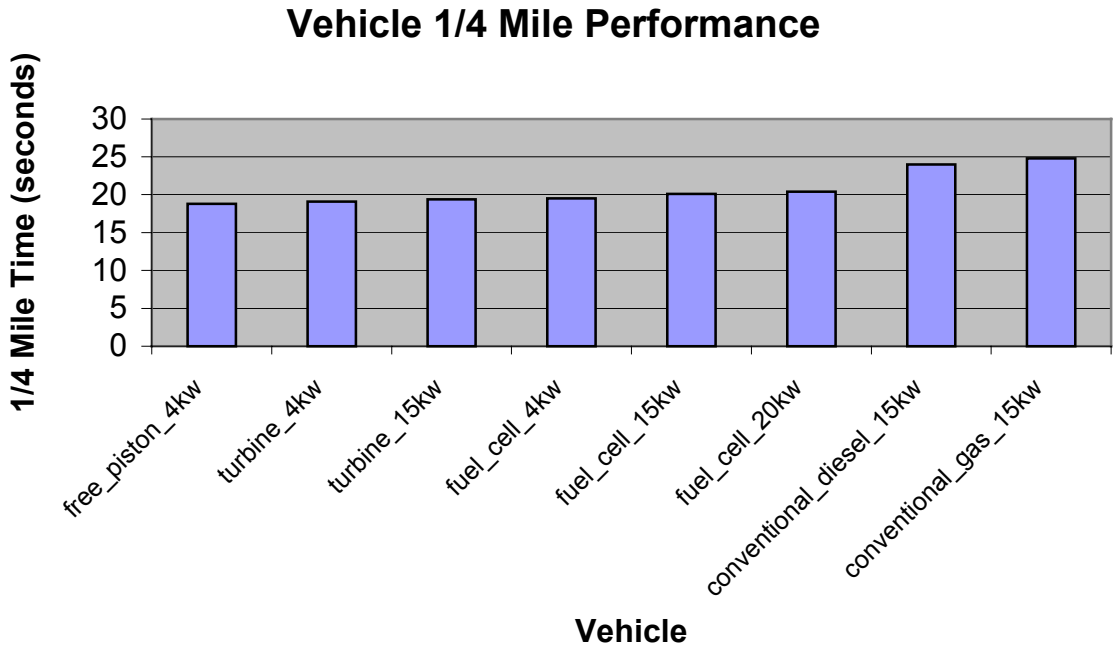

Figure 13: Vehicle Quarter Mile Performance.

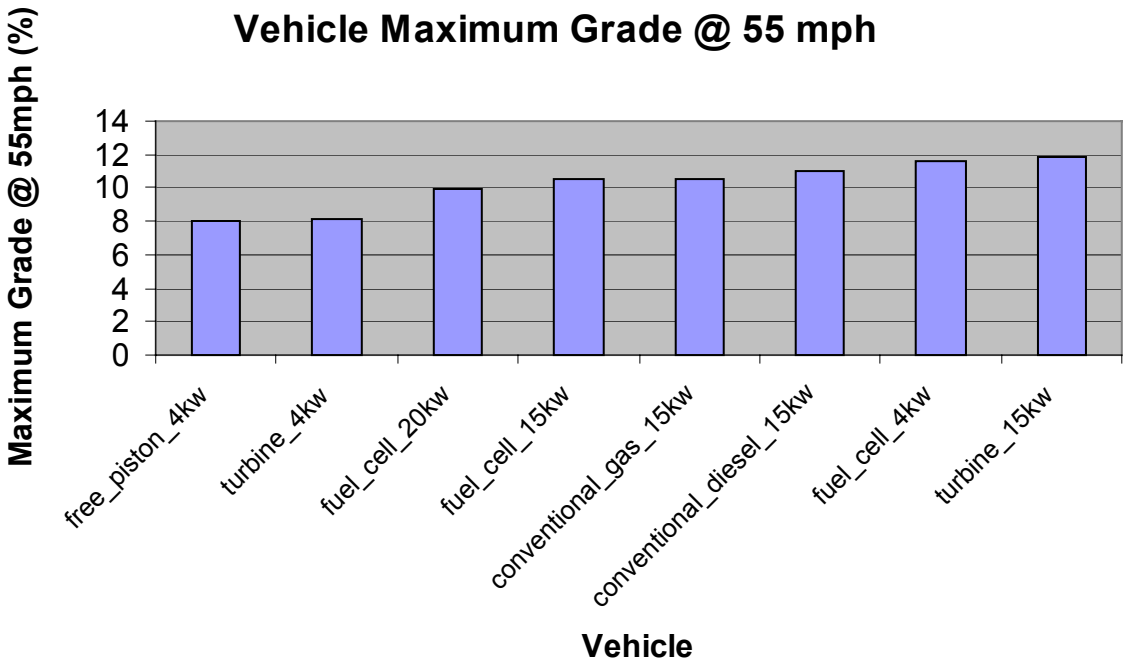

Figure 14: Vehicle Maximum Grade at 55 mph.

Discussion

The concept of a single occupancy vehicle for commuters leads to a compact and lightweight automobile. As a result, utilizing high efficiency drive trains leads to impressive fuel economy combined with spirited performance in both city and urban highway driving, as can be seen in Figures 10 thru 14. The model shows that it is possible to double the fuel economy of the SOV relative to a conventional drive train.

Of the three advanced hybrid drivetrains the low power auxiliary power unit appears to offer the most. Both microturbines and fuel cells are likely to be very expensive converters for some time, and keeping them small should help hold down cost, at least in the case of the fuel cell. While the free piston generator is likely to be much less expensive, it is in its infancy of development and has a long way to go. However, the experiments conducted in this program have shown that the high efficiency potential can be achieved even at power levels as low as 2 kilowatts; the lower limit is yet to be established.

Based on the modeling and experiments conducted here the following conclusions are offered:

1. The free piston engine can be a serious contender for low power hybrid drivetrains – A combination of high efficiency, low cost production and high theoretical and experimentally verified potential. The ability to operate on a variety of fuels is a plus. The demonstration of a complete prototype has not yet been accomplished.

2. The fuel cell is the most technologically advanced power supply – but at high cost and low demonstrated robustness. The need for hydrogen as a fuel is a severe handicap in the near term.
3. The microturbine does not appear to offer the efficiency potential to compete with the previous two hybrid concepts.
4. The SOV concept with a conventional drivetrain offers many of the advantages of the hybrid vehicles with few of the drawbacks. On a liters per mile basis, 160 MPG versus 90 MPG is not saving that much fuel (19 liters - 5 gallons) in 1,000 miles driving.

Summary

Both conventional and advanced series hybrid drivetrains have been modeled for application to a single occupancy vehicle. One of the advanced prime movers, the free piston generator, has been shown experimentally to have high efficiency potential at a 2 kilowatt power output size. However, for the purpose of establishing the viability of single occupancy vehicles as commuter machines, conventional drivetrain technology appears to offer the best combination of demonstrated reliability, low cost and acceptable efficiency.

This page intentionally left blank

Appendix A

Homogeneous Charge Compression Ignition with a Free Piston: A New Approach to Ideal Otto Cycle Performance

Abstract

Sandia National Laboratories has been investigating a new, integrated approach to generating electricity with ultra low emissions and very high efficiency for low power (30 kW) applications such as hybrid vehicles and portable generators.

Our approach utilizes a free piston in a double-ended cylinder. Combustion occurs alternately at each cylinder end, with intake/exhaust processes accomplished through a two stroke cycle. A linear alternator is mounted in the center section of the cylinder, serving to both generate useful electrical power and to control the compression ratio by varying the rate of electrical generation. Thus, a mechanically simple geometry results in an electronically controlled variable compression ratio configuration.

The capability of the homogeneous charge compression ignition combustion process employed in this engine with regards to reduced emissions and improved thermal efficiency has been investigated using a rapid compression expansion machine. Eight different fuels, including propane, natural gas, hydrogen, methanol, n-pentane, hexane, n-heptane, and isooctane have been used at low equivalence ratio (~ 0.35) and initial temperatures of 25°C, 50°C and 70°C.

The results indicate that the cycle thermal efficiency can be significantly improved (56% measured) relative to current combustion systems, while low NO_x emissions are possible (<10 PPM). HC and CO emissions must be controlled through some aftertreatment technology. The primary cause of this high conversion efficiency is nearly constant volume combustion at high compression ratio (~ 30:1).

Introduction

Sandia National Laboratories is developing a combustion-driven generator set for application in both transportation and stationary power systems. Our goal is to maximize the thermal efficiency at a particular operating point while releasing essentially zero emissions. The operating principle is to ignite and burn lean (fuel/air equivalence ratio (~ 0.4) homogeneous charge mixtures, thereby improving the indicated thermal efficiency [1], while reducing the peak cylinder temperatures to a level where essentially no NO_x is formed [2]. Based on measured engine-out emissions from a rather conventional, but optimized for hydrogen, four stroke cycle spark ignition engine, we project compliance with the California Air Resources Board's (CARB)

proposed standard for equivalent zero emissions vehicles, when the generator set is integrated into a series type hybrid power train for a standard size automobile [2].

The motivation for the present work derives from the fact that internal combustion (IC) engines used in these types of applications have operating requirements that are significantly different from IC engines used in conventional drivetrain applications. Here, shaft power is not required since all of the output power is converted to electrical energy. As well, the engine can be operated within a narrow speed/power output range, cycling on and off as needed. Finally, engine operation can be controlled automatically so that throttle response is unimportant.

In addition to operational differences, there are powerful incentives for advanced IC engines to have the capability of operating efficiently on a multitude of fuels (both conventional and unconventional) without significant hardware modification. Such versatile engines would help to improve the viability of futuristic fuels such as methanol and hydrogen.

The combination of these unique operating parameters and the results from our spark ignition engine program, has led us to formulate a new design specific to electric power applications, which is different from conventional configurations. The primary goals considered in this development are high energy conversion efficiencies and stringent emissions compliance. The result is an engine that operates on a unique homogeneous charge compression ignition (HCCI) combustion process using a free piston geometry.

The remainder of this paper develops the rationale behind the new concept, details the experimental apparatus used to validate the combustion approach, presents the results gathered utilizing a variety of different fuels, and discusses the significance of the data to date. Future papers will detail further developments of the generator concept.

Background

Advanced hybrid vehicles and stationary power systems will no doubt be powered by electrical generators capable of high conversion efficiencies and extremely low exhaust emissions. Fuel cells are generally considered to be ideal devices for these applications where hydrogen or methane is used as the fuel. In the near term however, the extensive development of the IC engine, and the existence of repair and maintenance industries associated with piston engines provide strong incentives to remain with this technology until fuel cells are proven reliable and cost competitive. In addition, while the fuel cell enjoys high public relations appeal, it seems possible that it may not offer significant efficiency advantages relative to an optimized combustion system. In light of these factors, the capabilities of internal combustion engines have been reviewed.

In regards to thermodynamic efficiency, the Otto cycle theoretically represents the best option for an IC engine cycle. This is due to the fact that the fuel energy is converted to heat at constant volume when the working fluid is at maximum compression. This combustion condition leads to the highest possible peak temperatures, and thus the highest possible thermal efficiencies.

Edson [3] analytically investigated the efficiency potential of the ideal Otto cycle using compression ratios (CR) up to 300:1, where the effects of chemical dissociation, working fluid thermodynamic properties, and chemical species concentration were included. He found that even as the compression ratio is increased to 300:1, the thermal efficiency still increases for all of the fuels investigated. At this extreme operating point for instance, the cycle efficiency for isooctane fuel at stoichiometric ratio is over 80%.

Indeed it appears that no fundamental limit exists to achieving high efficiency from an internal combustion engine cycle. However, many engineering challenges are involved in approaching ideal Otto cycle performance in real systems, especially where high compression ratios are utilized.

Caris and Nelson [4] investigated the use of high compression ratios for improving the thermal efficiency of a production V8 spark ignition engine. They found that operation at compression ratios above about 17:1 did not continue to improve the thermal efficiency in their configuration. They concluded that this was due to the problem of non constant volume combustion, as time is required to propagate the spark ignited flame.

In addition to the problem of burn duration, other barriers exist. These include the transfer of heat energy from the combustion gases to the cylinder walls, as well as the operating difficulties associated with increased pressure levels for engines configured to compression ratios above 25:1 [5,6]. Still, finite burn duration remains the fundamental challenge to using high compression ratios.

The goal of emissions compliance further restricts the design possibilities for an optimized IC engine. For example, in order to eliminate the production of nitrogen oxides (NO_x), the fuel/air mixture must be homogeneous and very lean at the time of combustion [7,8]. (It is subsequently possible to use oxidation catalyst technologies to sufficiently control other regulated emissions such as HC and CO.) Homogeneous operation precludes Diesel-type combustion, and spark ignition operation on premixed charges tends to limit the operating compression ratio due to uncontrolled auto-ignition, or knock. As well, very lean fuel/air mixtures are difficult, or impossible to spark ignite.

On the other hand, lean charges have more favorable specific heat ratios relative to stoichiometric mixtures, and this leads to improved cycle thermal efficiencies. Since three way catalysts are no longer required in this emissions controlling scheme, the operating equivalence ratio does not need to be precisely controlled, as it does in conventional stoichiometric operation. Equivalence ratio is defined here as the ratio of the actual fuel/air ratio to the stoichiometric ratio.

A New Combustion Approach

Homogeneous charge compression ignition combustion could be used to solve the problems of burn duration, and allow ideal Otto cycle operation to be more closely approached. In this combustion process a homogeneous charge of fuel and air is compression heated to the point of auto-ignition. Numerous ignition points throughout the mixture can ensure very rapid combustion [7]. Very low equivalence ratios (~ 0.3) can be used since no flame propagation is required. Further, the useful compression ratio can be increased as higher temperatures are required to auto-ignite weak mixtures [8].

HCCI operation is unconventional, but it is not new. As early as 1957 Alperstein, et al. [11] experimented with premixed charges of hexane and air, and n-heptane and air in a Diesel engine. They found that under

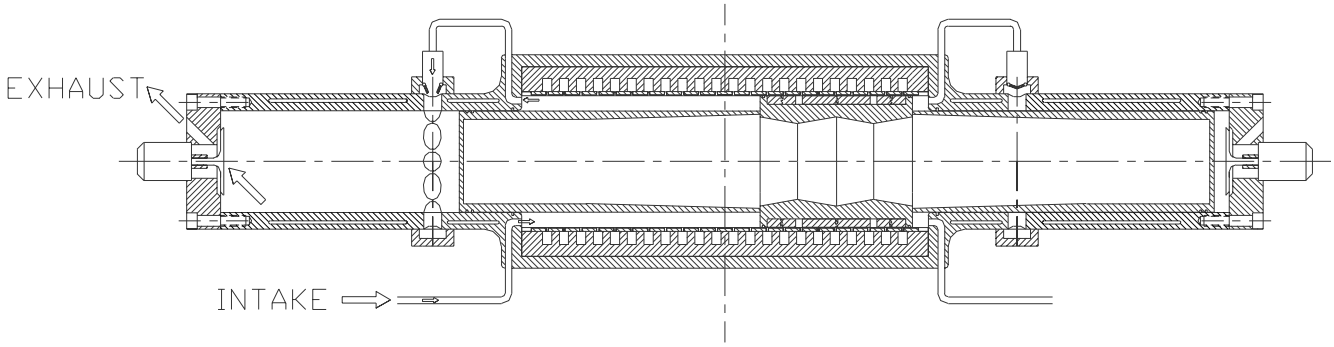

Figure A1: Free piston linear alternator.

certain operating conditions their single cylinder engine would run quite well in a premixed mode with no fuel injection whatsoever.

In general, HCCI combustion has been shown to be faster than spark ignition or compression ignition combustion. And much leaner operation is possible than in SI engines, while lower NO_x emissions result.

Most of the HCCI studies to date however, have concentrated on achieving smooth releases of energy under conventional compression conditions (CR ~ 9:1). Crankshaft driven pistons have been utilized in all of these previous investigations. Because of these operating parameters, successful HCCI operation has required extensive EGR and/or intake air preheating. Conventional pressure profiles have resulted [12,13].

In order to maximize the efficiency potential of HCCI operation much higher compression ratios must be used, and a very rapid combustion event must be achieved. Recent work with higher compression ratios (~21:1) has demonstrated the high efficiency potential of the HCCI process [14,15].

Engineering Configuration

The free piston linear alternator illustrated in Figure 1 has been designed in hopes of approaching ideal Otto cycle performance through HCCI operation. In this configuration, high compression ratios can be used and rapid combustion can be achieved.

The linear generator is designed such that electricity is generated directly from the piston's oscillating motion, as permanent magnets fixed to the piston are driven back and forth through the alternator's coils. Combustion occurs alternately at each end of the piston and a modern two-stroke cycle scavenging process is used. The alternator component controls the piston's motion, and thus the extent of cylinder gas compression, by efficiently managing the piston's kinetic energy through each stroke. Compression of the fuel/air mixture is achieved inertially and as a result, a mechanically simple, variable compression ratio design is possible with sophisticated electronic control.

The use of free pistons in internal combustion engines has been investigated for quite some time. In the 1950's, experiments were conducted with free piston engines in automotive applications. In these early designs, the engine was used as a gasifier for a single stage turbine [16,17]. More recent developments have integrated hydraulic pumps into the engine's design [18,19].

Several advantages have been noted for free piston IC engines. First, the compression ratio of the engine is variable; this is dependent mainly on the engine's operating conditions (e.g., fuel type, equivalence ratio, temperature, etc.). As a result, the desired compression ratio can be achieved through modification of the operating parameters, as opposed to changes in the engine's hardware.

An additional benefit is that the mechanical friction can be reduced relative to crankshaft driven geometries since there is only one moving engine part. Also, combustion seems to be faster than in conventional slider-crank configurations. Further, the unique piston dynamics (characteristically non-sinusoidal) seem to improve the engine's fuel economy and NO_x emissions by limiting the time that the combustion gases spend at top dead center (TDC) (thereby reducing engine heat transfer and limiting the NO_x kinetics). Finally, free piston engines are usually capable of operating on a variety of fuels.

The combination of the HCCI combustion process and the free piston geometry is expected to result in significant improvements in the engine's thermal efficiency and its exhaust emissions. The following advantages should be found:

1. For a given maximum piston velocity, the free piston arrangement is capable of achieving a desired compression ratio more quickly than a crankshaft driven piston configuration. This point is illustrated in Figure 2 where the piston position profiles of both configurations are plotted. The reduced compression time should result in higher compression of the premixed charge before the onset of auto-ignition.

2. High compression ratio operation is better suited to the free piston engine since the piston develops compression inertially, and as such there are no bearings or kinematic constraints that must survive high cylinder pressures or the high rates of pressure increase (shock). The use of low equivalence ratios in the HCCI application should further reduce the possibility of combustion chamber surface destruction [20,21].

3. The free piston design is more capable of supporting low equivalence ratio operation, and the correspondingly low IMEP levels due to the reduction in mechanical friction.

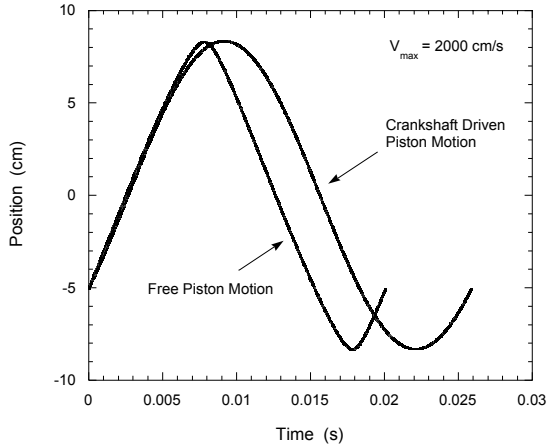

Figure A2: Piston position vs. time.

Combustion Experiments

While several new concepts are brought together in this generator design, it is the use of the free piston, HCCI combustion system that is the most significant. In order for the generator to be proven as a true advancement in IC engine technology, and to be able to compete with projected fuel cell capabilities, it is critical that the potential for high thermal efficiency and extremely low emissions be realized. To determine the achievable efficiencies and emissions reduction capabilities of the combustion system a series of experiments were conducted using a wide range of fuels.

A free piston, rapid compression-expansion machine (RCEM) has been used for the initial testing. The RCEM consists of a double-ended cylinder and a double-ended free piston, where the enclosed piston is allowed to move freely along the cylinder's axis. In this device, the combustion process is isolated from the rest of the engine cycle. The details of the RCEM and its operation can be found in the Appendix; however, a brief description of the combustion experiments is presented here.

Fuel/air mixtures of eight different fuels were tested using various initial temperatures where the energy density of the fuel/air charge was fixed. The eight fuels included propane, natural gas, hydrogen, methanol, n-pentane, hexane, n-heptane, and isooctane. The natural gas was composed of 93.13% methane, 3.2% ethane, 0.7% propane, 0.4% butane, 1.2% carbon dioxide, and 1.37%

nitrogen by volume. An energy density of 1.15 kJ/L ±4% at STP was used for this study. This was based on previous work with hydrogen in a modified spark ignition IC engine where the goal was to minimize the combustion temperatures, and thus the NO_x emissions [2]. The individual fuel/air equivalence ratios were adjusted to meet this energy value and are listed in Table 1. Initial charge temperatures of approximately 25°C, 50°C, and 70°C were used depending on the ease of autoigniting the mixture at the lower temperatures. For each different testing condition a range of compression ratios was investigated, where these were also adjusted depending on the fuel/air mixture's auto-ignition characteristics.

The metrics by which different experimental points are compared are the indicated thermal efficiency and the output emissions levels. The thermal efficiency was calculated by measuring both the pressure in the combustion chamber and the displacement of the piston. The network was integrated over the compression and expansion strokes. Since the combusted gas is not fully expanded through the expansion stroke of the piston (as discussed in the Appendix), the full potential of the thermodynamic cycle was determined by extrapolating both the piston position and the cylinder pressure data. This was done by matching the expansion line slope on a logarithmic pressure-volume diagram, as shown in Figure 3.

The NO_x, HC, and CO concentrations of the combusted gases were measured using continuous exhaust gas emissions analyzers. Since only a small quantity of gas sample was available for each data point, modified measuring techniques were developed. These are also detailed in the Appendix.

Experimental Results

The experimental results are presented in the following format. For each fuel/air mixture a logarithmic pressure

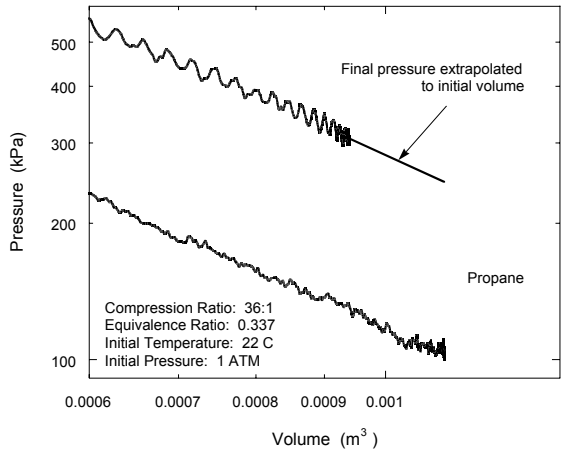

Figure A3: Log pressure vs. log volume.

vs. volume curve is plotted. These plots enable visualization of the rapidity of the combustion process, and the similarity to constant volume combustion conditions. Next, the thermal efficiency and emissions data are plotted versus the compression ratios investigated. The results of the test runs are summarized in Table 1, where the ranges of efficiencies and emissions are given.

For each testing condition (i.e., fuel/air equivalence ratio and initial temperature), the critical compression ratio, defined as the compression ratio required for TDC auto-ignition, is approximately fixed. Top dead center auto-ignition is where combustion occurs just as the piston reverses direction. TDC auto-ignition was easily discernable for the fast burning fuels like propane and hydrogen, however, such a definition was impossible for the slower burning fuels like n-pentane and hexane.

Compression ratios less than the critical compression ratio led to late ignition points (i.e., ignition after the piston passed TDC) or to no combustion at all. Compression ratios greater than the critical values seemed to simply over-compress the combusted gases, as in the case of the rapid burning fuel mixtures, or ensured further oxidation of the fuel, as in the case of n-pentane, hexane, and n-heptane and air mixtures.

The results for propane are presented first. Figure 4 plots the log pressure vs. log volume curve for a near TDC auto-ignition point. Here the equivalence ratio was 0.337 and the initial temperature 22°C. The compression ratio for this trace was 36:1. In this plot the piston position and pressure traces were smoothed using a binomial method to remove noise; this is consistent throughout the paper. The smoothing process, however, did not affect the efficiency calculations presented later.

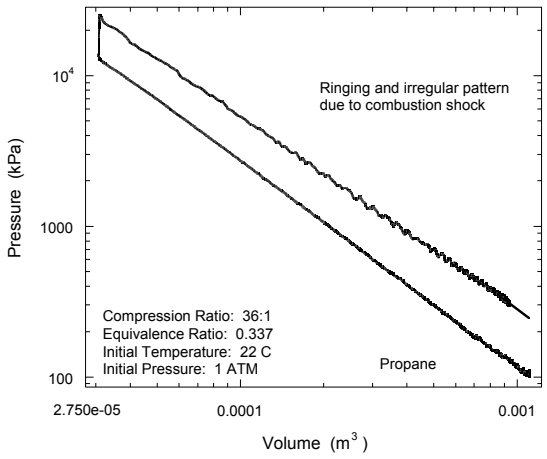

Figure A4: Log pressure vs. log volume.

In Figure 4 the similarity to the constant volume combustion process is evident. The rapidity of the HCCI process for this mixture is also illustrated in Figure 5 where the pressure vs. time curve

is plotted. Auto-ignition occurs just at TDC and the duration of combustion is approximately 50 ?s. As can be seen, the piston has hardly moved during this time.

Noticeable in Figures 4 and 5 is the intensity of combustion. The burning event is so rapid that considerable ringing is generated in the pressure and displacement records (this accounts for the sawtooth pattern and other irregularities in the figures). The vibration of the experimental apparatus due to combustion is further discussed in detail in the Appendix.

Table A1: Experimental Results.

Fuel	phi	T_{ini}	CR	$_{nTH}$	NO_x	HC	CO
Propane	0.337	22, 54°C	34-70:1	50-60 %	< 15 PPM	100-800 PPM	300-800
Natural	0.365	23, 67	30-54	50-55	10-130	600-2000	250-800
Hydrogen	0.319	22, 49,	17-50	40-55	1-550	< 25	< 120
Methanol	0.330	25	38-70	54-58	15-45	~ 600	300-800
n-Pentane	0.335	25	23-36	47-50	< 10	900-1050	800-1050
Hexane	0.336	26	19-34	40	< 5	1000-2000	1000-2500
n-Heptane	0.334	24	16-47	10-40	< 5	2000-4500	900-3000
Isooctane	0.321	25, 70	16-74	30-55	1-70	800-1050	300-3000

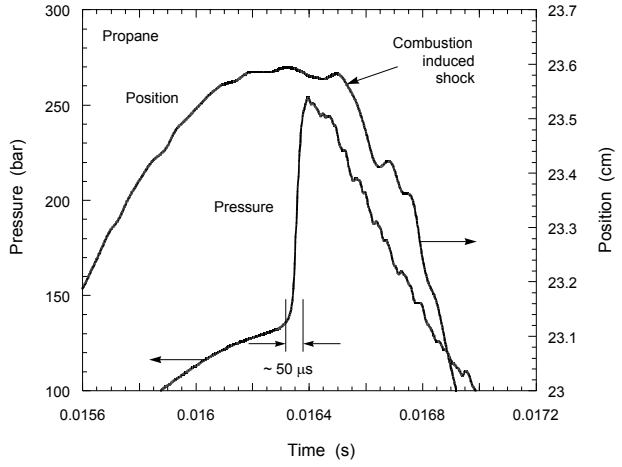

Figure A5: Pressure and piston position vs. time near TDC.

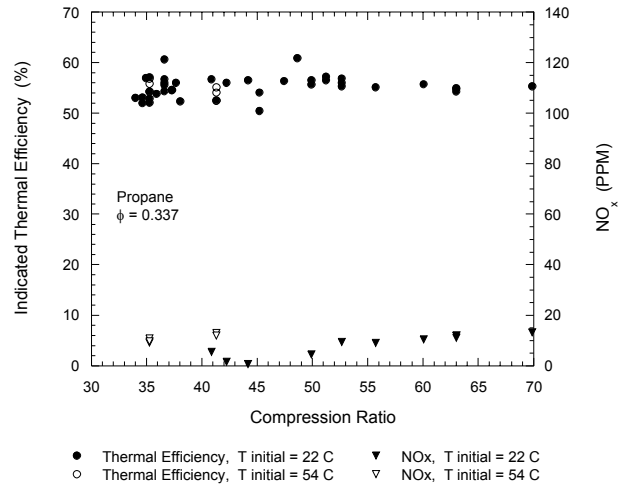

Figure A6: Indicated thermal efficiency and NO_x emissions vs. compression ratio.

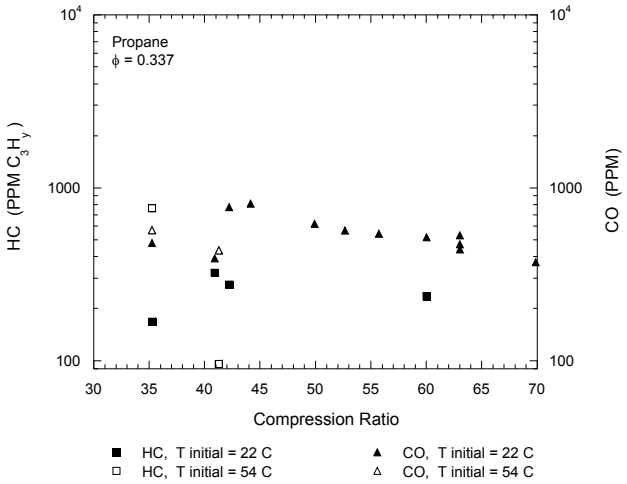

Figure A7: HC and CO emissions vs. compression ratio.

Figure 6 gives the efficiency and NO_x levels as a function of compression ratio. Some of the NO_x emissions data are missing due to lost gas samples or the use of the combusted gases for analysis of gas leakage (as explained in the Appendix).

For an initial temperature of 22°C, auto-ignition of the propane/air mixture first occurs at a compression ratio of about 34:1. The calculated efficiencies are somewhat scattered but fairly steady after this point, falling between 50% and 60%. The tests performed using an initial temperature of 57°C are consistent with these results. The NO_x emissions levels are all below 15 PPM, increasing slightly with increased compression. The increase in NO_x was expected as the cylinder gases are compressed to higher temperatures after combustion.

Figure 7 plots the unburned hydrocarbon and carbon monoxide emissions as a function of compression ratio. Some of the HC and CO emissions data are also missing. Here the hydrocarbon emissions are reported as parts per million of C_3H_y.

With increasing compression there seems to be little pattern to the change in HC emissions, while the CO emissions tend to decrease with increased compression. The HC emissions range from 100 to 800 PPM, and the CO emissions vary from 300 to 800 PPM.

Figures 8, 9 and 10 give the log pressure vs. log volume, thermal efficiency and NO_x vs. compression ratio, and HC and CO emissions vs. compression ratio, respectively, for natural gas at an equivalence ratio of 0.365. Initial temperatures of 23°C and 67°C were used.

From Figure 8 it is evident that near constant volume combustion is possible with this fuel mixture. The duration of combustion in this case is approximately 65 micro seconds. This is slower than the propane/air mixture, but still relatively fast.

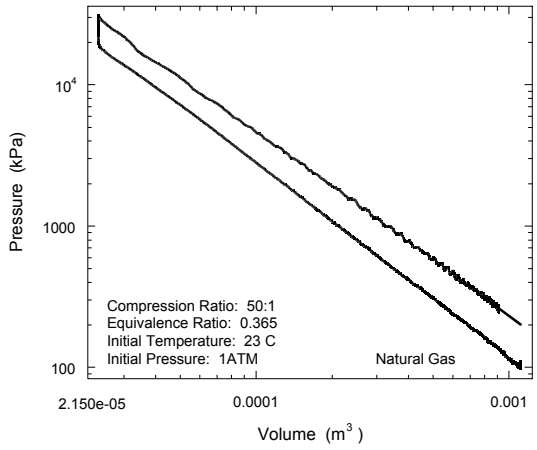

Figure A8: Log pressure vs. log volume.

The minimum compression ratio required for auto-ignition is much higher than that required for propane. At an initial temperature of 23°C late auto-ignition first occurs at about 44:1, and at an initial temperature of 67°C the critical compression ratio is approximately 30:1. The thermal efficiency is fairly constant for both test conditions over the range of compression ratios investigated. There is less scatter in these points probably due to the refinement in the experimental procedure; typical results are about 54%. The NO_x data show a more defined increasing trend with compression ratio, while the HC and CO emissions both decrease with compression ratio for each of the temperatures investigated.

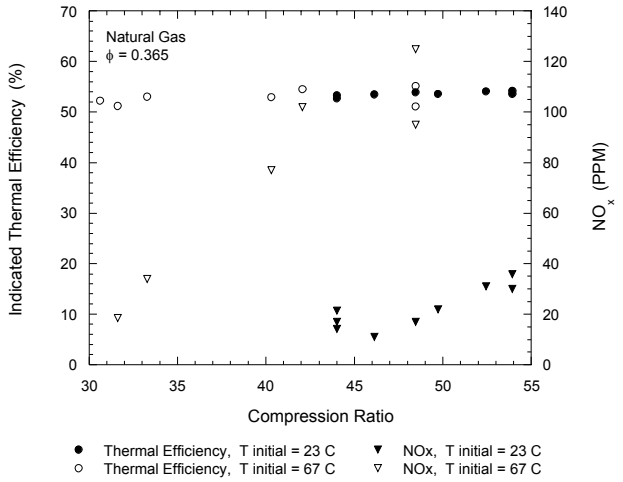

Figure A9: Indicated thermal efficiency and NO_x emissions vs. compression ratio.

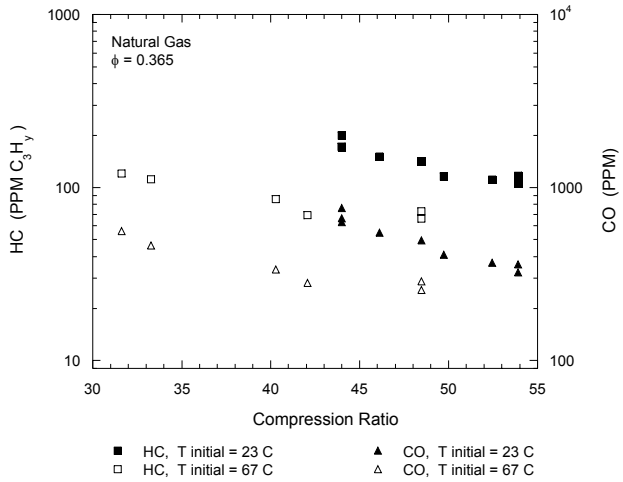

Figure A10: HC and CO emissions vs. compression ratio.

Further oxidation of the cylinder gases seems to be the cause of the decrease in HC and CO emissions. Increased initial temperature only slightly affects the emissions levels.

It should be noted that the scales for the efficiency and emissions plots are the same as those for the propane/air mixture. It can be seen that the NO_x and HC emissions for natural gas are higher than those for propane, however the CO emissions levels are comparable.

Figures 11, 12, and 13 show the results for hydrogen. In these runs an equivalence ratio of 0.319 was used at initial temperatures of 22°C, 49°C, and 68°C. Figure 11 illustrates the near constant volume combustion process for this fuel/air mixture at an initial temperature of 22°C. The

duration of combustion is only 20 micro seconds, the shortest combustion time recorded for any of the fuels tested.

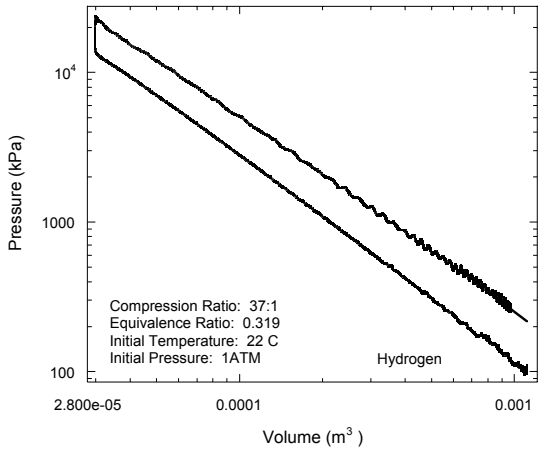

Figure A11: Log pressure vs. log volume.

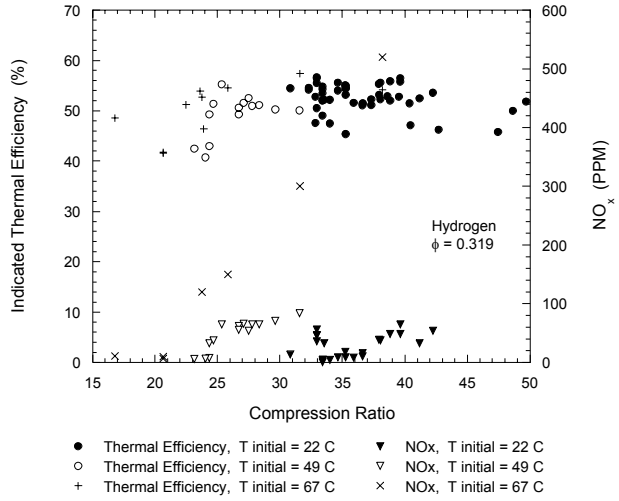

Figure A12: Indicated thermal efficiency and NO_x emissions vs. compression ratio.

The minimum compression ratios required for combustion are 30:1, 22:1, and 17:1 for initial temperatures of 22°C, 48°C, and 68°C, respectively. A significant amount of scatter is present in the efficiency points due to the fact that hydrogen was the first fuel tested.

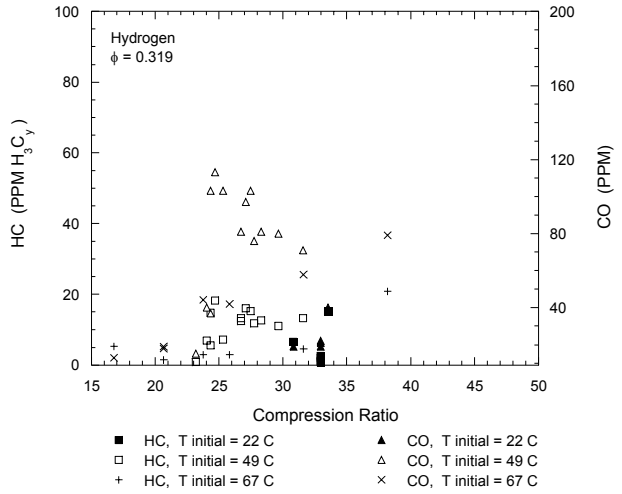

Figure A13: HC and CO emissions vs. compression ratio.

There seems to be little pattern to the change in efficiency with increased compression after TDC auto-ignition and only a small variation with changes in the starting temperature, even though the critical compression ratio is significantly affected.

The NO_x emissions are greater (a maximum of 530 PPM at an initial temperature of 67°C) than both the propane and natural gas mixtures, where the scale in Figure 12 is significantly increased. The NO_x levels for hydrogen also increase with compression of the cylinder charge after TDC combustion.

The HC and CO emissions data presented in Figure 13 represent the background emissions levels found in the system. These emissions are possibly due to contamination of the combustion chamber by piston ring lubricant oxidation, where this is discussed in the Appendix. (Ring lubricant oxidation could also be a source of error in the efficiency calculations for both hydrogen and propane fuels, where this would indicate higher than expected thermal efficiencies.) The hydrocarbon levels are below 20 PPM, and the carbon monoxide levels below 120 PPM.

The methanol test data is presented in Figures 14, 15 and 16. An equivalence ratio of 0.330 was used at an initial temperature of 25°C. From Figure 14, it is seen that near constant volume combustion is also possible with methanol. The duration of combustion is approximately 80 micro seconds, and the critical compression ratio about 35:1.

The indicated efficiencies range from 54-58% with a slight increase with compression ratio. The NO_x emissions also increased slightly with compression, where the peak value was 43 PPM. The HC and CO emissions levels are comparable to the levels seen with propane, and the CO concentrations decrease with over-compression after TDC combustion.

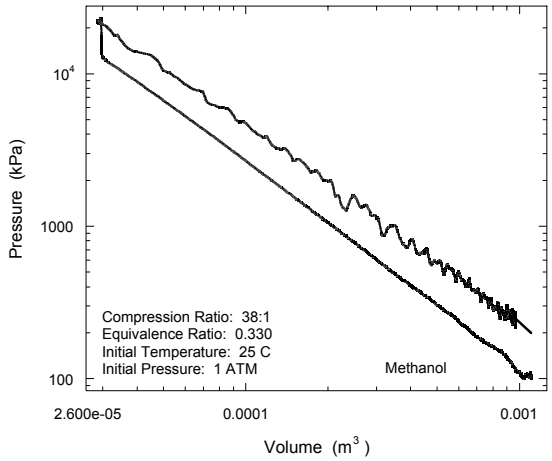

Figure A14: Log pressure vs. log volume.

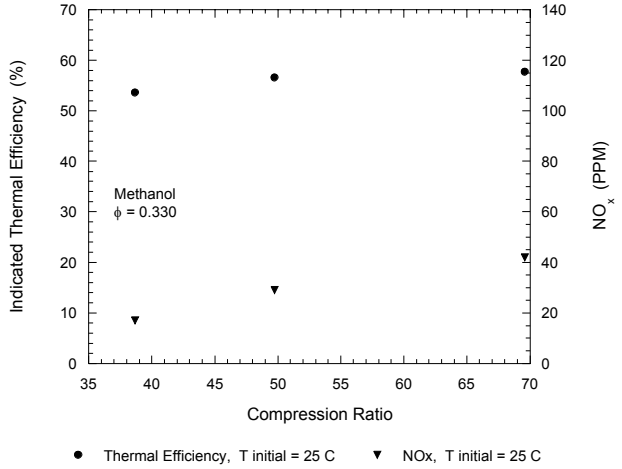

Figure A15: Indicated thermal efficiency and NO_x emissions vs. compression ratio.

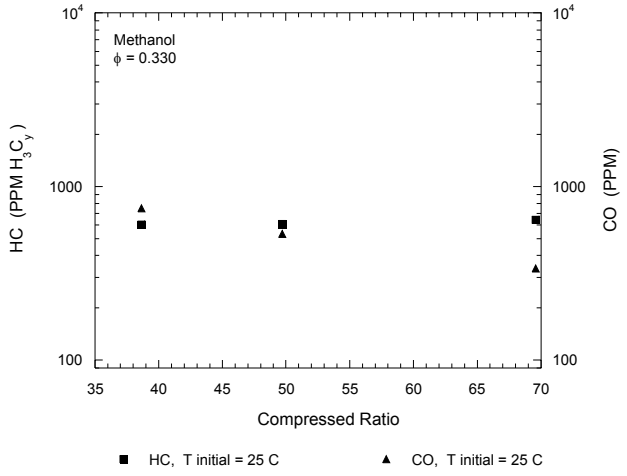

Figure A16: HC and CO emissions vs. compression ratio.

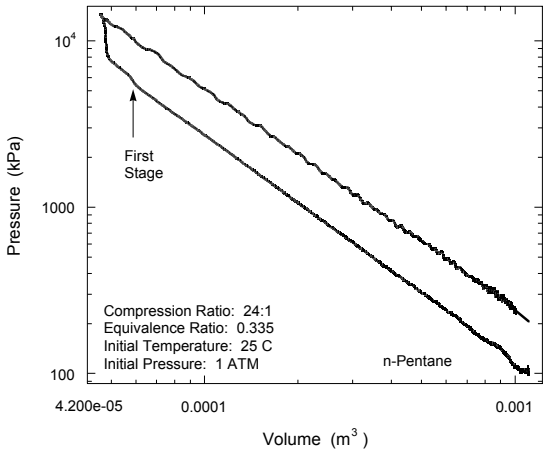

Figure A17: Log pressure vs. log volume.

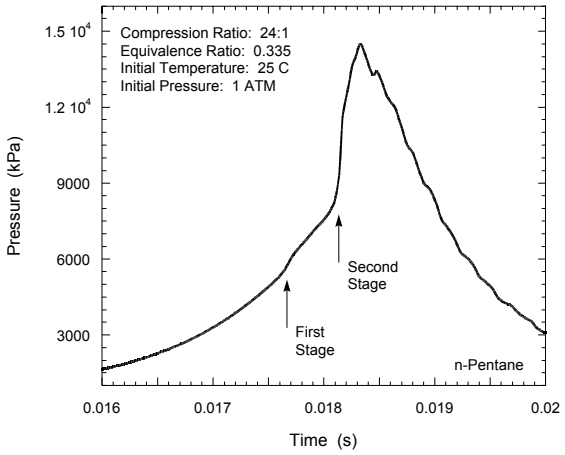

Figure A18: Pressure vs. time.

The results from the n-pentane tests are presented in Figures 17-20. An equivalence ratio of 0.335 was used at an initial temperature of 25°C.

From Figure 17 it is evident that this fuel does not burn in a near constant volume process. Two stages of combustion are clearly discernable from this plot. The first stage of fuel decomposition occurs at a compression ratio of about 18:1, and further compression is required to more completely oxidize the fuel.

The second stage, or point of major heat release occurs at approximately 23:1. This two stage process is much slower than the HCCI processes previously seen, taking approximately 600 micro seconds to complete.

The two stages of auto-ignition combustion are illustrated in Figure 18 where the pressure vs. time curve for this data point is plotted. The nature of this two-stage HCCI process has been previously reported in (22) where a rapid compression machine has been used to investigate the auto-ignition characteristics of various fuels.

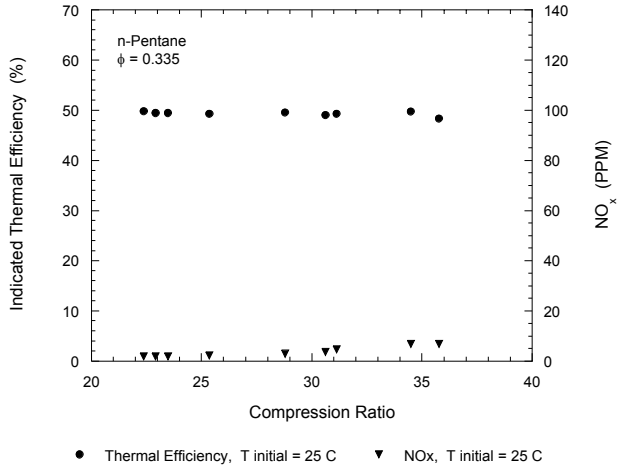

Figure A19: Indicated thermal efficiency and NO_x emissions vs. compression ratio.

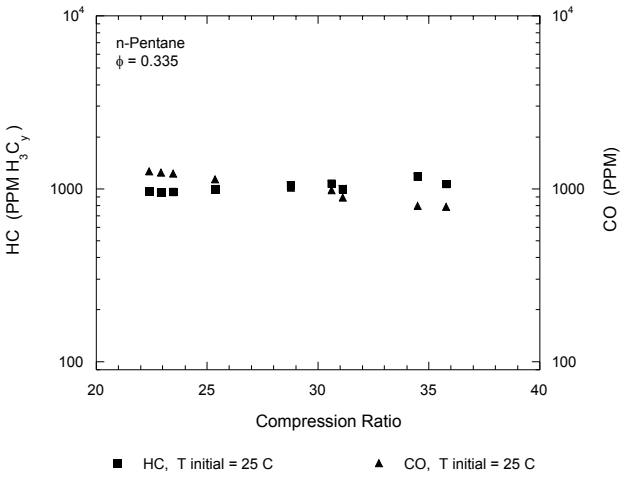

Figure A20: HC and CO emissions vs. compression ratio.

The efficiency calculations in Figure 19 exhibit a steady behavior with increasing compression, however, they are generally lower than the results from the previous fuels.

The NO_x and HC emissions only slightly increase with compression and range from less than 10 PPM and 900-1050 PPM, respectively. The CO emissions decrease slightly from about 1050 to 800 PPM with compression, where these concentrations are comparable to the other fuels.

The results for hexane are presented in Figures 21, 22, and 23. An equivalence ratio of 0.336 and an initial temperature of 25°C were used. Hexane also exhibited two-stage type HCCI combustion. Again, near constant volume combustion was impossible, with the duration of combustion about 600 micro seconds.

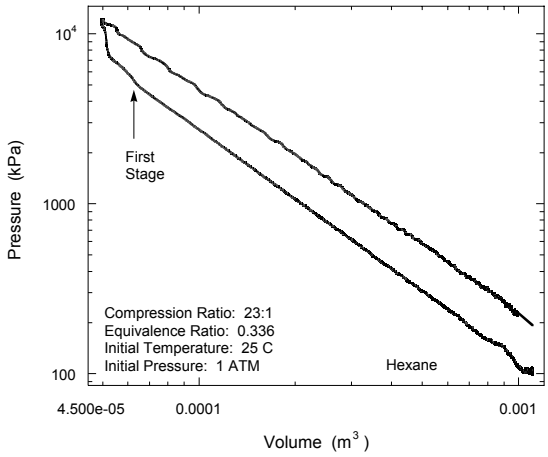

Figure A21: Log pressure vs. log volume.

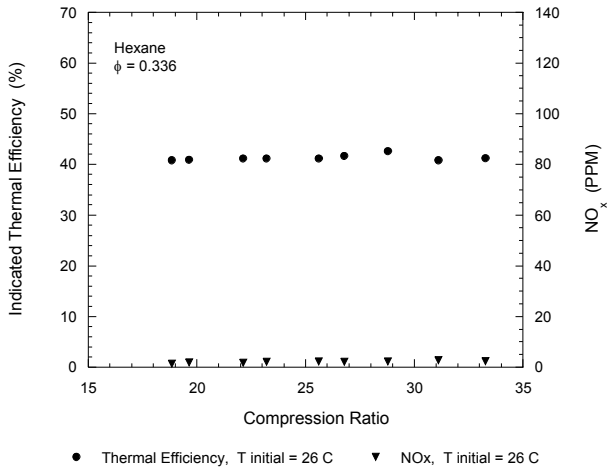

Figure A22: Indicated thermal efficiency and NO_x emissions vs. compression ratio.

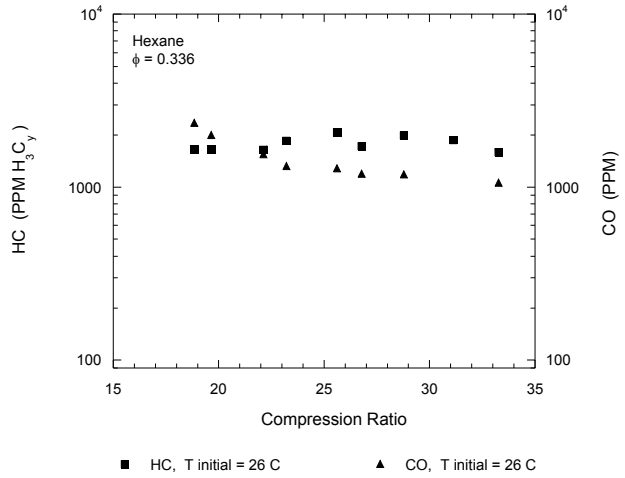

Figure A23: HC and CO emissions vs. compression ratio.

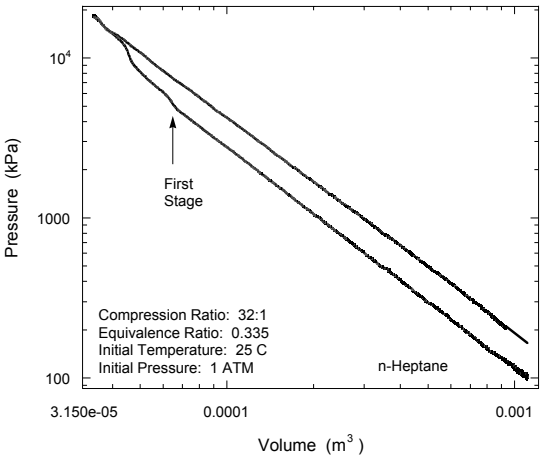

Figure A24: Log pressure vs. log volume.

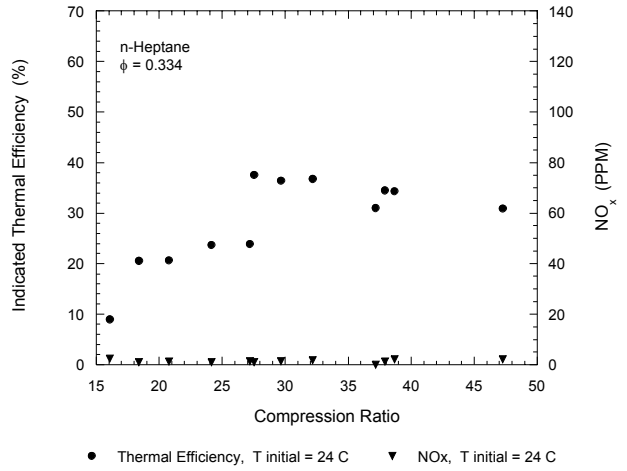

Figure A25: Indicated thermal efficiency and NO_x emissions vs. compression ratio.

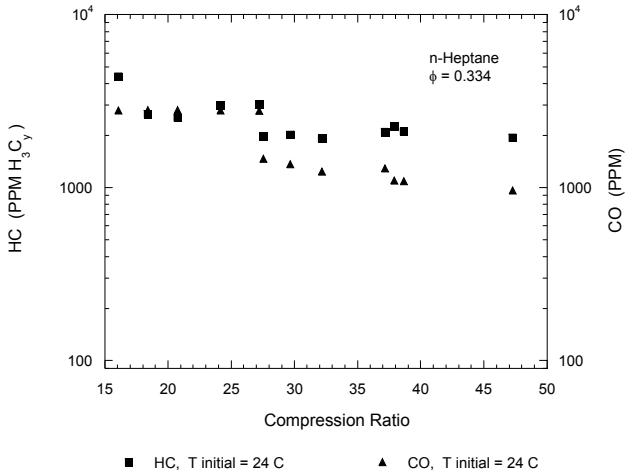

Figure A26: HC and CO emissions vs. compression ratio.

The efficiency and NO_x and HC emissions data are steady with compression ratio, while the CO emissions decrease. However, the results indicate that the HCCI process did not completely oxidize the fuel. The efficiency and NO_x are low (40% and <5 PPM, respectively), while the HC and CO emission are high (1000-3000 PPM) with respect to the other fuels.

Figures 24, 25, and 26 show the results for n-heptane. An equivalence ratio of 0.334 and an initial temperature of 24°C were used. It is evident that the HCCI combustion process for n-heptane also proceeds in two stages.

The efficiency results from Figure 25 indicate that at low compression ratios some reaction of the fuel occurs, however, even at compression ratios near 50:1 it seems as if combustion does not go to completion. The emissions data further support this conclusion. An increased initial temperature may improve the combustion conditions, however, this was not investigated.

The final data set is for isooctane, shown in Figures 27, 28 and 29. An equivalence ratio of 0.321 was used at initial temperatures of 25 and 70°C. Isooctane, like propane and natural gas, burned in a single step process and at nearly constant volume, as can be seen in Figure 27. However, the efficiency and emissions data indicate that the combustion process did not go to completion when the initial temperature was 25°C.

Further testing at 70°C seemed to improve the combustion conditions where higher efficiencies and lower emissions resulted. The trends with compression ratio at this starting temperature are similar to natural gas. However, the thermal efficiency is still lower than the most efficient fuels.

Discussion

The purpose of the combustion experiments was to establish the potential for high efficiency and low emissions of the free piston, HCCI combustion process. The data presented here do that, illustrating that significant improvements relative to conventional technologies are possible.

Compared to ideal Otto cycles operating at standard compression ratios (12:1) and using stoichiometric mixtures (about the limit of today's SI engines with three-way catalysts), ideal Otto cycles operating on much higher compression ratios (30:1) and utilizing lean mixtures are capable of thermal efficiency improvements of near 40%. Our experiments show a similar improvement relative to contemporary engine performance (6) with fuels such as propane, hydrogen, and natural gas, where indicated efficiencies near 56% have been measured.

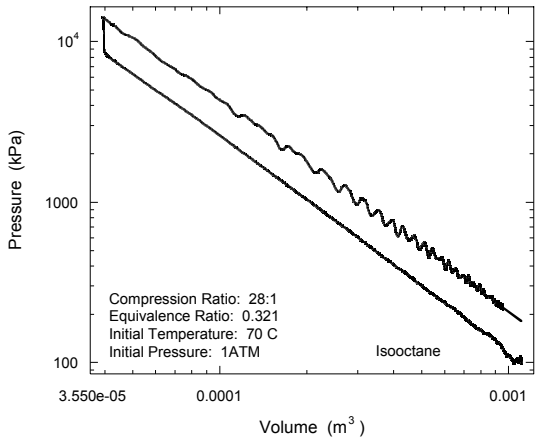

Figure A27: Log pressure vs. log volume.

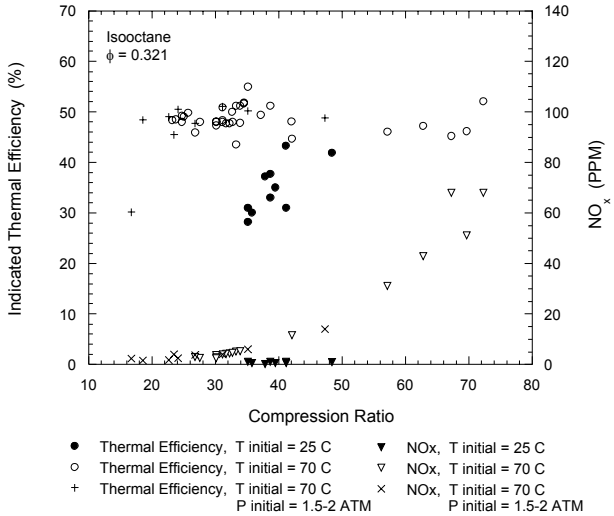

Figure A28: Indicated thermal efficiency and NO_x emissions vs. compression ratio.

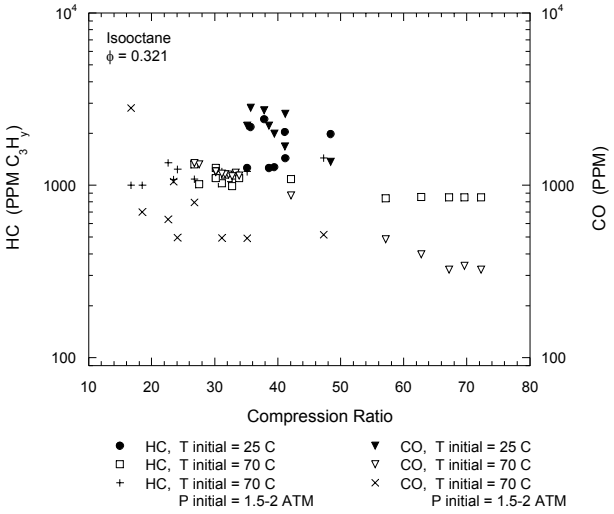

Figure A29: HC and CO emissions vs. compression ratio.

Comparison of these results to actual engine data, however, must be done with great caution since the intake and exhaust processes are not included, and the fuel/air mixture is completely homogeneous and quiescent before the compression stroke. However, the following trends are noted for the free piston, HCCI combustion process:

1. High compression ratio can be achieved at the time of combustion. While the initial temperature and fuel type have a strong effect on the compression ratio at which the combustion reactions begin, compression ratios above 30:1 seem achievable for practical operating conditions (e.g., inlet temperature, etc.). The data are unclear regarding efficiency improvements with increased compression ratio, though this

could be due to the range of starting temperatures used and the variation with the different fuels investigated.

2. The high rate of combustion in many cases approaches the constant volume combustion condition. This is especially true for the fuels which have a single stage combustion process (propane, natural gas, hydrogen, methanol, and isooctane).

3. Over-compression of the cylinder gases after auto-ignition occurs does not seem to significantly affect the cycle thermal efficiency. While it is possible that greater heat losses are balanced by an increase in the extent to which the fuel/air mixture reacts to completion, this effect cannot be large since the greatest heat release occurs earlier in the compression stroke. This seems to indicate that heat losses do not significantly increase with over-compression. This conclusion is justified by the fact that operation of the experiment without the piston and cylinder head insulation coatings resulted in an efficiency of only 5% less than the insulated runs.

4. NO_x emissions do increase with over-compression. This is due mainly to the increased temperatures that result, or the increased time that the cylinder gases spend at higher temperatures.

5. NO_x emissions can be sufficiently controlled by decreasing the equivalence ratio, since the problems of spark igniting ultra lean mixtures are not of concern in the HCCI combustion process. HC and CO emissions are present in varying degree, but increasing the initial temperature generally seems to reduce these emissions.

6. The auto-ignition characteristics of the fuels tested in these experiments varied widely, and as such the efficiency and emissions results differed significantly. As the data show, some fuels do not react completely, or react in two steps. Generally, higher initial temperatures and higher compression ratios were required to burn more of the fuel to completion. An additional factor that may affect the burning process, especially for the two stage fuels, is the rate of piston oscillation. This variable should be investigated in the future.

The oxidation catalyst performance on these emissions should be investigated in the future. An interesting possibility for emissions control would be to utilize 50% internal EGR (i.e. leave 50% of the combustion products in the cylinder) and add a stoichiometric fresh charge to the remaining cylinder volume. Such an operating strategy with a three-way catalyst could be very attractive. A test series investigating this option was performed with propane where the emissions after 4 cycles were measured. NO_x was 130 PPM, CO 1720 PPM and HC 360 PPM. The indicated thermal efficiency was 50%.

Current research with HCCI combustion in crankshaft driven engines have shown results similar to ours. Christensen et al [15] evaluated isooctane, ethanol and natural gas in a 1.6 liter displacement single cylinder research engine at a fixed 21:1 compression ratio, at a speed of 1000 RPM. Their efficiency results (not including the inlet/exhaust strokes) using similar equivalence ratios are over 50%.

This research raises the question as to the importance of the free piston geometry to this combustion concept. Certainly the lack of massive kinematic constraints is attractive for such high compression ratios, and the electronic control of compression ratio broadens the operating range. However, the increased compression ratio possible with the free piston at the time of combustion may not provide much advantage. In the future the performance of the combustion system using a free piston and a crankshaft driven piston under identical operating condition will be compared.

Finally, our work, as well as Christensen's, adds further credibility to the explanation of timing loss as the main cause for real cycle departure from ideal cycle performance as compression ratio is increased.

Summary

This paper presents the results of an investigation conducted to determine the effect of homogeneous charge compression ignition combustion of dilute fuel/air mixtures with a free piston on the cycle thermal efficiency and exhaust emissions. The investigation was conducted in a single stroke gas driven combustion experiment in which an initially quiescent, premixed fuel/air charge was compressed to the point of auto-ignition and then expanded. The cycle thermal efficiency was calculated from measurements of pressure and piston displacement, and the NO_x, HC, and CO emissions were measured on the combustion gases using continuous exhaust gas analyzers.

The results of this study have shown that significant improvements in indicated thermal efficiencies relative to spark ignition engine performance can be achieved. The results for propane and natural gas were approximately 56%. The primary cause of this high conversion efficiency is nearly constant volume combustion at high compression ratio.

In addition, this combustion approach controls NO_x formation by utilizing dilute mixtures, an approach not possible in spark ignition engines utilizing hydrocarbon fuels. Regulated emissions such as HC and CO must be controlled by exhaust gas aftertreatment.

Acknowledgements

This work was supported by the U. S. Department of Energy, the Office of Solar Thermal, Biomass Power and Hydrogen Technologies, and the Laboratory Directed Research and Development Program at Sandia National Laboratories. The authors gratefully acknowledge the technical assistance of David Zanini.

References

1. Edson, M. H. and Taylor, C. F., "The Limits of Engine Performance - Comparison of Actual and Theoretical Cycles," Digital Calculations of Engine Cycles, SAE Program in Technology, vol. 7, pp.65-81, 1964.

2. Van Blarigan, P., "Development of a Hydrogen Fueled Internal Combustion Engine Designed for Single Speed/Power Operation," SAE Paper 961690, 1996.

3. Edson, M. H., "The Influence of Compression Ratio and Dissociation on Ideal Otto Cycle Engine Thermal Efficiency," Digital Calculations of Engine Cycles, SAE Program in Technology, vol. 7, pp. 49-64, 1964.

4. Caris, D. F. and Nelson, E. E., "A New Look at High Compression Engines," SAE Transactions, vol. 67, pp. 112-124, 1959.

5. Overington, M. T. and Thring, R. H., "Gasoline Engine Combustion - Turbulence and the Combustion Chamber," SAE Paper 810017, 1981.

6. Muranaka, Y. T. and Ishida, T., "Factors Limiting the Improvement in Thermal Efficiency of S.I. Engine at Higher Compression Ratio," SAE Transactions, vol. 96, section 4, pp. 526-536, 1987.

7. Das, L. M., "Hydrogen Engines: A View of the Past and a Look Into the Future," International Journal of Hydrogen Energy, vol. 15, no. 6, pp. 425 - 443, 1990.

8. Van Blarigan, P. and Green, R., "NO_x Emission Data Verified in a Hydrogen Fueled Engine," Combustion Research Facility News, vol. 17, no. 4, January/February 1995.

9. Onishi, S., Jo, S. H., Shoda, K., Jo, P. D. and Kato, Satoshi, "Active Thermo-Atmospheric Combustion (ATAC) - A New Combustion Process for Internal Combustion Engines," SAE Paper 790501, 1979.

10. Karim, G. A. and Watson, H. C., "Experimental and Computational Considerations of the Compression Ignition of Homogeneous Fuel-Oxidant Mixtures," SAE Paper 710133, 1971.

11. Alperstein, M., Swim, W. B. and Schweitzer, P. H., "Fumigation Kills Smoke - Improves Diesel Performance," SAE Transactions, vol. 66, pp. 574-588, 1958.

12. Thring, R. H., "Homogeneous-Charge Compression-Ignition Engines," SAE Paper 892068, 1989.

13. Najt, P. M. and Foster, D. E., "Compression-Ignited Homogeneous Charge Combustion," SAE Paper 830264, 1983.

14. Christensen, M., Johansson, B., Amneus, P. and Mauss, F., "Supercharged Homogeneous Charge Compression Ignition," SAE Paper 980787, 1998.

15. Christensen, M., Johansson, B. and Einewall, P., "Homogeneous Charge Compression Ignition (HCCI) Using Isooctane, Ethanol and Natural Gas - A Comparison with Spark Ignition Operation," SAE Paper 972874, 1997.

16. Underwood, A. F., "The GMR 4-4 'Hyprex' Engine - A Concept of the Free-Piston Engine for Automotive Use," SAE Paper 570032, 1957.

17. Klotsch, P., "Ford Free-Piston Engine Development," SAE Paper 590045, 1959.

18. Baruah, P. C., "A Free-Piston Engine Hydraulic Pump for an Automotive Propulsion System," SAE Paper 880658, 1988.

19. Achten, P. A. J., "A Review of Free Piston Engine Concepts," SAE 941776, 1994.

20. Lee, W. and Schaefer, H. J., "Analysis of Local Pressures, Surface Temperatures and Engine Damages under Knock Conditions," SAE Transactions, vol. 92, section 2, pp. 511-523, 1983.

21. Maly, R. R., Klein, R., Peters, N. and Konig, G., "Theoretical and Experimental Investigation of Knock Induced Surface Destruction," SAE Transactions, vol. 99, section 3, pp. 99-137, 1990.

22. Park, P. and Keck, J. C., "Rapid Compression Machine Measurements of Ignition Delays for Primary Reference Fuels," SAE Paper 900027, 1990.

APPENDIX A.1

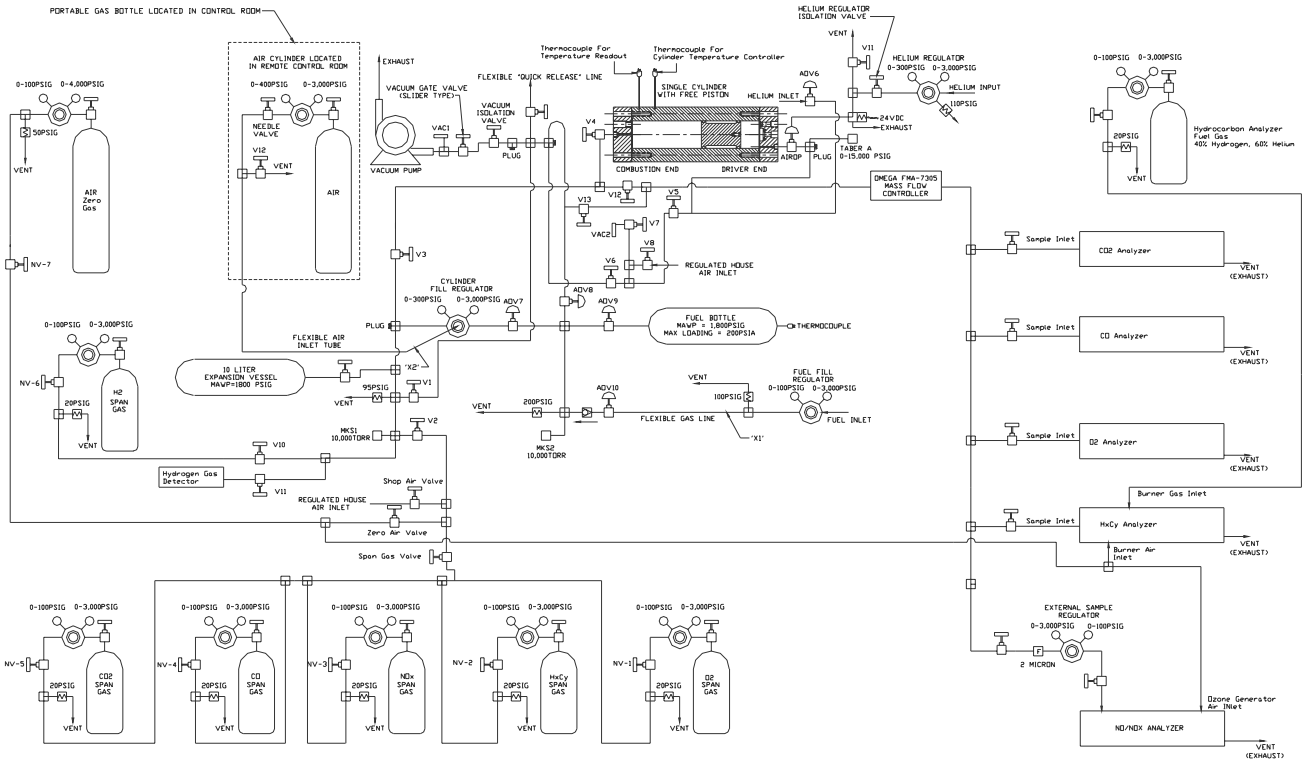

Figure A.1-1: Schematic of free piston combustion experiment.

RAPID COMPRESSION EXPANSION MACHINE - A schematic of the RCEM and the experimental setup is illustrated in Figure A.1. The RCEM uses high pressure helium gas to drive a double ended, free piston from one end of a double ended cylinder to the other. This driving motion compresses the initially quiescent fuel/air charge to the point of auto-ignition. As the combusted gases expand the piston is driven back through the cylinder recompressing the helium driver gas. The piston bounces a few times before coming to rest. The oscillating piston motion from a typical run is illustrated in Figure A.2. Here it can be seen that the piston does not fully return to its initial position due to the compression of the trapped helium gas.

The relevant specifications of the RCEM can be found in Table A.1. A detailed description of the machine's construction and operation follow.

Double-Ended Cylinder - The cylinder section was constructed of 6061-T6 aluminum with the dimensions of 35.56 cm length, 7.62 cm inside diameter, and 15.24 cm outside diameter. The cylinder bore was hard anodized and honed to a finish of 16-32 microinches. The body was wrapped with Briskheat electrical heating tape and covered with FiberFrax insulation to perform heated experiments.

Cylinder Heads - The front and back cylinder heads were constructed of 304 stainless steel. The front head (combustion chamber) contained access ports for two pressure transducers, two surface thermocouples, an air-operated pressure trap, and fuel loading. All pressure transducer holes were centered on a radius of 25 mm. The port for fuel loading was located in the center of the head. The back cylinder head contained access ports for one pressure transducer and the source driver gas. Both cylinder heads were wrapped with Briskheat electrical heating tape, over wrapped with ThermoTec insulation, and then covered with FiberFrax insulation.

Table A.1-1: Rapid Compression - Expansion Machine Specifications.

Bore (mm)	76.2
Stroke (mm)	254 max, 236 typical
Displacement (L)	1.076 typical
Cylinder	6061 aluminum, hard anodized
Cylinder Head	304 stainless steel
Piston	303 stainless steel
Maximum Piston Speed (cm/s)	1100 typical
Natural Oscillation Frequency (Hz)	40 typical

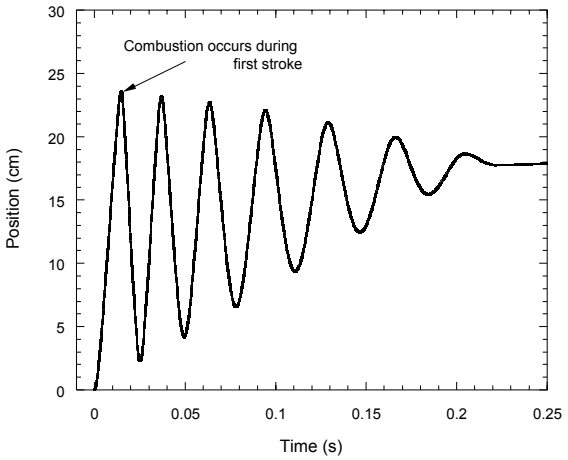

Figure A.1-2: Piston position vs. time.

Piston and Seals - The double ended piston was machined from 303 stainless steel to the dimensions of 11.05 cm length and 7.85 cm diameter. The mass of the piston, including the piston seals, was 2.89 kg.

In order to accurately quantify the thermal efficiency of the cycle it was important that the cylinder gases not be lost to leakage from the combustion chamber. In an effort to seal off the front chamber, three different seal configurations were used. These are described in detail below. The final combination represented the best option for the combustion experiment's operation, and produced the most consistent data.

In the first configuration each end of the piston was fitted with one ring seal. A Furon lip seal (part # 250-334-3307) was used in conjunction with a stainless steel expander spring. Additionally, a Teflon sleeve was attached to piston's midsection to improve the piston's movement inside the cylinder. Parker Teflon-impregnated o-rings (part #2-334-V848) were used in place of the Furon seals in some tests.

In the second configuration the piston was fitted with two seals located on the combustion chamber end, and one seal on the driver end. In this design a C. Lee Cook compression ring (part # 559648WGX) was used on the outer combustion chamber end, and behind that, a Furon lip seal (part # 250-334-3307). Here an o-ring was used in the place of the expander spring. On the driver end, a Furon lip seal was used with the stainless steel expander ring. In addition to these outer seals, two C. Lee Cook bronze-impregnated Teflon rider rings (part # 559647MFL) were fitted to the piston's midsection. Parker Teflon-impregnated o-rings were also used in place of the Furon ring on the combustion chamber end in later tests.

The third seal configuration used two seals on the combustion chamber end and one on the driver end. The outer combustion chamber seal used a Parker orange Teflon ring (part # S-5000-48), and behind that a Furon lip seal (part # 250-334-3307) with an o-ring expander second ring. On the driver end a Furon lip seal was used in conjunction with a stainless steel expander spring. In

this configuration, two C. Lee Cook bronze-impregnated Teflon rider rings were used. In later tests a Parker Teflon impregnated o-ring was used in place of the Furon seal on the combustion end.

Due to the changes in the piston/seal mass resulting from the different seal configurations, the piston's center section had to be machined so that the total piston/seal mass of 2.89 kg could be maintained.

Seal Lubrication - In early tests Parker silicone based Super-O-Lube was used to lubricate the o-rings. This lubricant however, was found to partially oxidize during the experimental runs. This was especially noticeable after the hydrogen and isooctane tests. Deposits were found on both the piston and cylinder head, and within the tubing leading to the emissions analyzers. Inaccurate readings of the exhaust emissions and fouled efficiency calculations resulted. The extent to which the emissions data were skewed can be seen in Figure 13, where the HC and CO emissions should have been null.

The use of seal lubrication was discontinued after this finding and the experimental apparatus fully cleaned.

Piston and Cylinder Head Coating - The piston crown and combustion chamber head were coated with Dow Corning Silastic J silicone in order to reduce the heat transfer between the cylinder gases and the combustion chamber surfaces. The details of the application procedure are described below.

The piston and cylinder head were first glass bead blasted to roughen the surface, and then wiped with acetone to remove any contamination. The cylinder head was masked off with a 15.24 cm diameter round plastic adhesive sheet that had a 7.62 cm hole in the center. This mask was used to limit the area covered with Silastic J and to set the depth of the coating. Both parts were primed with Dow Corning P5200 adhesion promoter.

After the primer dried, the silicone was applied to both parts with a spatula. The silicone was also applied to an aluminum blank that had been treated with mold release. The blank had three small pins, each protruding 0.5mm from its surface which were used to maintain a gap between the piston and the blank.

The piston and cylinder head, and blank were then placed in a vacuum chamber to degas the Silastic J. The parts were removed from the vacuum chamber and the piston placed on the aluminum blank. The weight of the piston forced the excess from between the piston and the blank leaving the piston resting on the blank's pins. The coating on the cylinder head was leveled with the mask by drawing a straight edge across the surface.

Both parts were allowed to cure overnight with a final cure the next day in an oven at 60 C for four hours. The coating thickness was verified by slicing the coating from each part with a razor and measuring its thickness with a caliper.

Fuel Mixing - Both liquid and gaseous fuels were tested. For gaseous fuels a premixed charge storage bottle (10 liters) was evacuated to a pressure of 1 Torr or less, and then filled with the fuel to a desired pressure (calculated based on the fuel/air equivalence ratio). When this pressure was reached, the bottle was valved off and the contents allowed to achieve a stable temperature. Changes in the fuel's pressure were recorded, and then dry air was slowly added until the total fuel and air pressure reached the required value.

For liquid fuels two methods were used to mix the fuel and air. The first method used a direct cylinder injection technique while the other relied on the use of a premixed storage bottle. A brief description of each follows.

In the first method the combustion chamber was initially filled with dry air to atmospheric pressure and sealed off. The fuel loading port was opened and a small amount of fuel injected directly into the cylinder using a stainless steel syringe. The port was quickly closed and the mass of injected fuel measured on a Mettler AE-163 scale. The fuel was then allowed to completely evaporate. This process lead to variations in the fuel/air equivalence ratio between test runs so a new method of fuel loading was developed.

In the second method the premixed storage bottle was initially evacuated to a pressure of 1 Torr or less. A small container containing liquid fuel was then connected to the storage bottle housing and the fuel allowed to evaporate into the bottle and piping. Once the bottle pressure and temperature stabilized the bottle was valved off and the liquid fuel container removed. Dry air was added to the storage bottle until the desired equivalence ratio was reached. Care was taken to ensure that the fuel remained vaporized at room temperature.

Mass spectrometer analysis has verified the precision of each mixing method.

The RCEM was located in a high pressure test cell. The transfer of the combustible gas mixes from the 10 liter fuel/air tank to the experiment cylinder was done remotely, as was the addition of air to the fuel/air storage tank and the firing of the device.

Cylinder Charging - To fuel the experiment the piston was moved to its initial position at the back of the cylinder by use of vacuum and atmospheric pressures. The entire assembly was then evacuated to a pressure of 1 Torr or less, and the premixed fuel/air charge loaded through the fueling port to a cylinder pressure of about 760 Torr.

Piston Driving - The helium driver gas was remotely pumped up to the required driving pressure using a Newport Scientific Aminco pump. The driver gas pressure was typically 362,000-490,000 Torr, depending on the desired compression ratio (higher compression ratios required higher driver pressures). To dump the high pressure helium gas into the driver end of the cylinder, a specially modified Nupro bellows valve actuated with an Autoclave Engineers air operator (also driven by helium) was used. With this configuration the driver supply was quickly released into the back end of the cylinder. Data acquisition was triggered by the rising pressure in the driver end.

Pressure Measurement - The static magnitude of all low pressure gases was measured using two 10,000 Torr absolute pressure range MKS Barratrons, Type 390 HA heads with Type 270B display units achieving an accuracy of 0.05% of reading. High pressure gases (i.e., helium) were measured using Teledyne-Taber strain gauge transducers with an accuracy of 0.25% of full scale.

Dynamic pressures were measured using piezoelectric effect transducers. Pressure on the driver end was quantified with a Kistler Type 607 transducer coupled to a Kistler Type 5004 charge amplifier. The combustion end utilized two transducers. Kistler Type 7061A, 7063A, 7061B, 607L, and AVL Type QC42D-X were employed with Kistler Type 5010 and 5026 charge amplifiers. To improve the accuracy of the combustion pressure measurements the transducers were coated with Dow Corning Silastic J silicone compound. The application procedure was essentially the same as that used for the piston/cylinder head coating, and is described below.

Pressure data were recorded on three Nicolet 4094 digital oscilloscopes through 12 bit Type 4570 plug-ins, at a rate of 500,000 samples per second.

In order to ensure the accuracy of the combustion chamber pressure record, an additional Teledyne-Taber Type 2210 transducer was added to the cylinder head. This transducer was isolated from the combustion event through the use of an air-operated valve. The valve, initially closed, was opened during the first expansion stroke so that the final expansion pressure could be recorded. A Daytronic Type 3270 strain gage conditioner/indicator was used in conjunction with this transducer.

A comparison of the Teledyne-Taber transducer record to the Kistler and AVL records indicated that the AVL unit matched the Teledyne-Taber record better.

Pressure Transducer Coating - The procedure for applying the Silastic J thermal coating to the pressure transducers is described here. The application procedure for the Kistler and AVL pressure transducers was very similar to the piston/head coating procedure. The transducers were first glass bead blasted to roughen the surface, and then wiped with acetone to remove any contamination. The transducers were coated with Dow Corning P5200 adhesion promoter; this promoter was found to work equally well for the plain style stainless steel face transducers and the TiN coated transducers.

After the primer dried the transducers were threaded into a setup fixture and locked with their faces 0.5mm below the surface of the fixture. Silastic J was then applied to the transducers with a spatula. The transducers were placed in a vacuum chamber to degas the Silastic J. The transducers and fixture were then removed from the chamber and the Silastic J leveled by pulling a razor across the surface of the setup fixture. The transducers were then allowed to cure overnight with a final cure the next day in an oven at 60 C for four hours. After the transducers cooled they were removed by slicing the Silastic J around the transducer face and unthreading them from the fixture. The coating thickness was verified by coating one transducer without first priming it. This allowed the cured Silastic J to be peeled from the transducer and its thickness measured with a caliper.

Displacement Measurement - The piston displacement was measured using a Data Instruments FASTAR Model FS5000HP inductive transducer. Data were recorded on a fourth Nicolet 4094 digital oscilloscope at a rate of 200,000 samples per second.

Vibration Measurement - The vibration of the rapid compression-expansion machine was measured using two Endevco Model 2250A M1-10 accelerometers mounted on the back end cylinder head. One accelerometer recorded vibrations along the cylinder's axis, while the other recorded movement in the transverse direction. Both accelerometers were connected to Unholtz-Dickie Mod D22 series charge amplifiers and data were recorded on a fifth Nicolet 4094 digital oscilloscope through 12 bit Type 4570 plug-ins, at a rate of 500,000 samples per second.

The physical vibration of the RCEM was thought to be a source of noise in the pressure and displacement data records as seen in Figure 5. This was confirmed by analyzing the vibration history of the machine.

Figure A.3 plots the transverse acceleration of the machine along with the position-time trace. It can be seen that the machine shakes considerably after the combustion event. This motion was concluded to be responsible for the jaggedness of the position data, and the sawtooth shape of the pressure record.

Exhaust Emissions - Due to the small quantity of combusted gas available, a series of steps were taken to maximize the analysis of the combustion products. After each run the cylinder gas was fed through an Omega Engineering, Inc. Model FMA 7305 flow controller and into the analyzer manifold. Separate

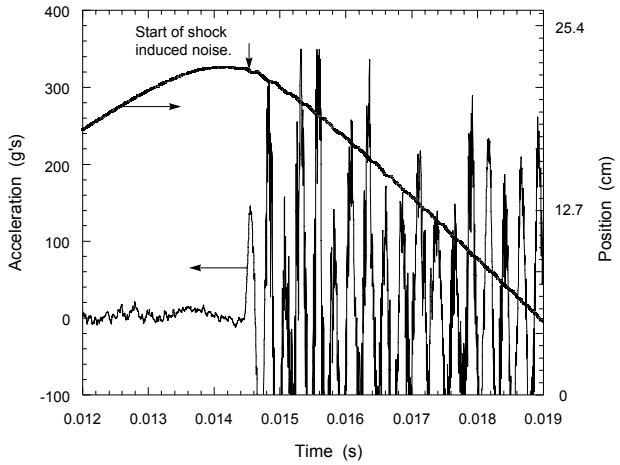

Figure A.1-3: RCEM lateral acceleration and piston position vs. time.

valves were used to control the flow into each emissions analyzer. The feeds were split from the flow meter and only one analyzer used at a time. The free piston-cylinder arrangement maintained a constant back pressure on the combusted gases.

Analysis of the NO_x, CO, CO_2, and HC concentrations was achieved by alternating the flow through each emissions analyzer. The response time for each detector was quantified through the calibration procedure.

Emissions Calibration - Each of the analyzers used was calibrated in the same manner. First, appropriate zero and span gases from compressed gas cylinders were sent through each analyzer via the flow meter manifold described above. After each analyzer was calibrated, the span gas was reintroduced to the analyzer to determine the response time required to achieve consistent readings.

This procedure was then repeated, but this time with the zero and span gas sources located in the piston-cylinder device. The response time for data acquisition in this manner was also noted.

NO_x Measurement - A Rosemont Analytical Model 951A NO_x analyzer was employed for NO and NO_x measurement. This analyzer was calibrated using a 6.7 parts per million (PPM) NO span gas. Since only one cylinder's worth of combustion products was available for analysis, the bypass flow was eliminated, and the burned gases pumped directly through the analyzer.

CO Measurement - A Rosemont Analytical Model 880A Non-Dispersive Infrared CO analyzer was employed for CO measurements. This analyzer was calibrated using an 801 PPM CO span gas.

CO_2 Measurement - A Rosemont Analytical Model 880A Non-Dispersive Infrared CO_2 analyzer was employed for CO_2 measurements. This analyzer was calibrated using a 3.89% CO span gas.

Unburned Hydrocarbon Measurement - A Rosemont Analytical Model 400A flame ionization hydrocarbon analyzer was employed for unburned HC measurements. This analyzer was calibrated using a 110 PPM propane-in-nitrogen background span gas. In this device the bypass flow was also eliminated, and the burned gases pumped directly through the analyzer.

Combustion Gas Analysis - In order to quantify leakage of the gases from the cylinder during the test sequence, the combusted gases were periodically examined using pressure-volume-temperature (PVT) analysis. In this post test procedure the combustion products were expanded into a larger measurement tank (10 liters) to a pressure of approximately 80 Torr to ensure that all the water vaporized. Due to the small quantity of gas available only a PVT test or emissions analysis could be performed.

Distribution :

1	MS 9108	M. Hardwick	08214
1	MS 9661	P. Van Blarigan	08214
4	MS 9661	N. Paradiso	08119
1	MS 9661	D. Zanini	08118
1	MS 9105	C. Scholz	08119
1	MS 0839	V. Gupta	16000
1	MS 9409	S. Eisenbies	08731
3	MS 9018	Central Technical Files, 8945-1	
1	MS 0899	Technical Library, 9616	
1	MS 9021	Classification Office, 8511/Technical Library, MS 0899, 9616	
1		DOE/OSTI via URL (sent electronically by R&A)	

This page intentionally left blank